This project has received funding from the European Union's
Horizon 2020 research and innovation programme under Grant Agreement N°763990

UPWARDS

Deliverable D6.6

Results from study cases applying integrated simulation framework

WP	6	Integrated System Simulation and Knowledge Extraction
Task	6.6	HPC-Framework Machine Learning

Dissemination level[1]	PU	Due delivery date	31/06/2022
Nature[2]	D	Actual delivery date	10/10/2022

Lead beneficiary	Fraunhofer ITWM
Contributing beneficiaries	All partners

Document Version	Date	Author	Comments[3]
1.7	10.10.2022	Benjamin Adrian	Final submit
1.6	06.10.2022	Sophie Le Bras	Revised product names
1.5.	04.10.2022	Benjamin Adrian	Edited conclusion
1.4	03.10.2022	Paul Bonnet	Edited Study Case 3
1.3	30.09.2022	Sophie Le Bras	Edited Study Case 2
1.2	29.09.2022	Alberto Cardona	Edited Study Case 1
1.1	08.09.2022	Balram Panjwani	Reviewed Study Case 1
1.0	01.07.2022	Benjamin Adrian	Initial draft version

[1] Dissemination level: **PU** = Public. **PP** = Restricted to other programme participants (including the JU). **RE** = Restricted to a group specified by the consortium (including the JU). **CO** = Confidential. only for members of the consortium (including the JU)

[2] Nature of the deliverable: **R** = Report. **P** = Prototype. **D** = Demonstrator. **O** = Other

[3] Creation. modification. final version for evaluation. revised version following evaluation. final

Deliverable abstract

This document reports examples of how a park could be analyzed. The analysis can be used for existing parks or parks that have yet to be planned. Deliverable 6.6 describes three case studies that were conducted using the integrated simulation framework developed in the Upwards project (refer to Figure 1). In case study 1 the effect of changing the yaw misalignment (difference between the wind direction and the nacelle position of the turbine) of certain turbines on wake, turbulence, productivity and fatigue is considered. Both an onshore and an offshore park are used for this examination. Case study 2 deals with the effect of yaw misalignment in an onshore park on the noise level in the neighborhood. The results are used in Deliverable 7.3 where they are analyzed with respect to stakeholder needs. In case study 3 the influence of slender design of large blades of a 15 MW turbine is studied. Here the effects on wind structure interaction, non-linear bending, buckling and complex structural stresses are considered.

Deliverable Review

	Reviewer #1:			Reviewer #2:		
	Answer	Comments	Type *	Answer	Comments	Type *
1. Is the deliverable in accordance with						
(i) The Description of Work?	☐ Yes ☐ No		☐ M ☐ m ☐ a	☐ Yes ☐ No		☐ M ☐ m ☐ a
(ii) The international State of the Art?	☐ Yes ☐ No	Not applicable for this deliverable	☐ M ☐ m ☐ a	☐ Yes ☐ No	Not applicable for this deliverable	☐ M ☐ m ☐ a
2. Is the quality of the deliverable in a status						
(i) That allows it to be sent to European Commission?	☐ Yes ☐ No		☐ M ☐ m ☐ a	☐ Yes ☐ No		☐ M ☐ m ☐ a
(ii) That needs improvement of the writing by the originator of the deliverable?	☐ Yes ☐ No		☐ M ☐ m ☐ a	☐ Yes ☐ No		☐ M ☐ m ☐ a
(iii) That needs further work by the Partners responsible for the deliverable?	☐ Yes ☐ No		☐ M ☐ m ☐ a	☐ Yes ☐ No		☐ M ☐ m ☐ a

* Type of comments: M = Major comment; m = minor comment; a = advice

Table of content

Table of Figures

1. Introduction

When planning a wind park there are lots of aspects to consider. Where to place the turbines? What size of turbine is optimal? How should they be controlled? Those are just some of the questions that have to be answered. The final park should maximize power, minimize stress in order to decrease fatigue and minimize the produced noise to increase acceptance of the park. Since complex coupled phenomena influence those properties, it is not easy to find optimal parameters. However, the integrated simulation framework developed in the Upwards project can help answer those questions. This deliverable presents examples of how a park could be analyzed. The analysis can be used for existing parks or parks that have yet to be planned.

Deliverable 6.6 describes three case studies that were conducted using the integrated simulation framework developed in the Upwards project (refer to Figure 1). The goal is to study complex coupled phenomena of wind energy engineering.

In Study Case 1 the effect of changing the yaw misalignment (difference between the wind direction and the nacelle position of the turbine) of certain turbines on wake, turbulence, productivity and fatigue is considered. Both an onshore and an offshore park are used for this examination. The results could for example be used to design a yaw-based controller.

Study Case 2 deals with the effect of yaw misalignment in an onshore park on the noise level in the neighborhood. The results are used in Deliverable 7.3 where they are analyzed with respect to stakeholder needs. This can help increase the acceptance of wind parks.

In Study Case 3 the influence of slender design of large blades of a 15 MW turbine is studied. Here the effects on wind structure interaction, non-linear bending, buckling and complex structural stresses are considered.

1.1. Contributions to project objectives

The concept underpinning UPWARDS is to develop an integrated HPC simulation framework of high-fidelity simulation codes capable of performing high-fidelity wind turbine and wind energy park simulations including wind flow, fully coupled fluid structure interaction, progressive damage, and noise propagation.

The conduction of study cases based on the HPC integrated simulation platform contributes to the project objectives of the Upwards agreement:

Objective 1 (O1): Establish a high-fidelity multi-physics, mechatronic and multi-scale simulation framework for wind turbines that enables integrated modelling of wind flow, mechanical movements, structural/control dynamics, and stresses with a level of details that today only is achievable in modelling of isolated phenomena.

b) State of the simulation tools and models for wind flow from atmospheric to turbine scale, rotor noise generation and propagation and composite material damage models. Methods and protocols will be developed to link these tools to enable efficient sequential modelling of all scales and physics.

Objective 2 (O2): Define a virtual prototype of a 15 MW horizontal axis wind turbine to utilize in simulation under realistic conditions.

UPWARDS will define a virtual prototype of a 15MW horizontal axis wind turbine including the description of aerodynamic and structural design, transmission, generator and control system. The purpose of the virtual prototype is to serve as study case to ensure that the developed simulation tools perform as required and enable generation of realistic and relevant simulation result for knowledge extraction and further exploitation.

Objective 3 (O3): Generate in-depth knowledge of important wind turbine related physical phenomena through high fidelity simulations.

High fidelity simulations of important wind turbine related phenomena will be performed using the high fidelity simulation framework described in O1 to exploit and increase the understanding of their physical behaviour and interaction. The virtual prototype described in O2 will be utilized as a base for the simulations. In addition, existing or virtual wind turbine parks at relevant onshore and offshore locations will be applied as study cases. State of the art data mining methods will be used to extract and structure relevant information from the data.

Objective 5 (O5):

Distribute and enable further use of the generated knowledge, data, and results

b) Quantitative data describing key features of the simulation study cases performed addressing O4 including details of virtual prototype

1.2. Document Outline

This documentation provides a description and analysis of the conducted study cases.

In Section 2.1 to Section 2.3 the first Study Case is described, and its results analysed. First the onshore park is considered. We simulate and analyse two different wind directions for this park. A description of the effects of yaw misalignment on wake follows. Then the effect of the yaw misalignment on the produced power is considered. Further the resulting fatigue of the turbines is studied. After this detailed analysis of the onshore park, we consider the offshore park. Here we focus on the produced power and show similar results to the ones obtained for the onshore park. This indicates that the results regarding the fatigue from the onshore park can be extended easily to offshore parks.

In Section 2.4, Study Case 2 is considered which deals with the effects of yaw misalignment on the noise level in the neighbourhood. We concentrate on the onshore park Høg-Jæren (https://www.vindenergi.no/project/hog-jaeren-vindpark). First the noise fields are considered. Then the noise level at one specific point is examined. A farm is situated at that point. Thus, the manipulation of the yaw misalignment to decrease noise at that point is of interest.

Section 3.5 corresponds to Study Case 3, where the influence of slender design of large blades of a 15 MW turbine within a park situation is studied. By using a combined simulation on fluid and mechanic dynamics the interaction effects on wind and structure, i.e., non-linear bending, buckling and complex structural stresses are considered.

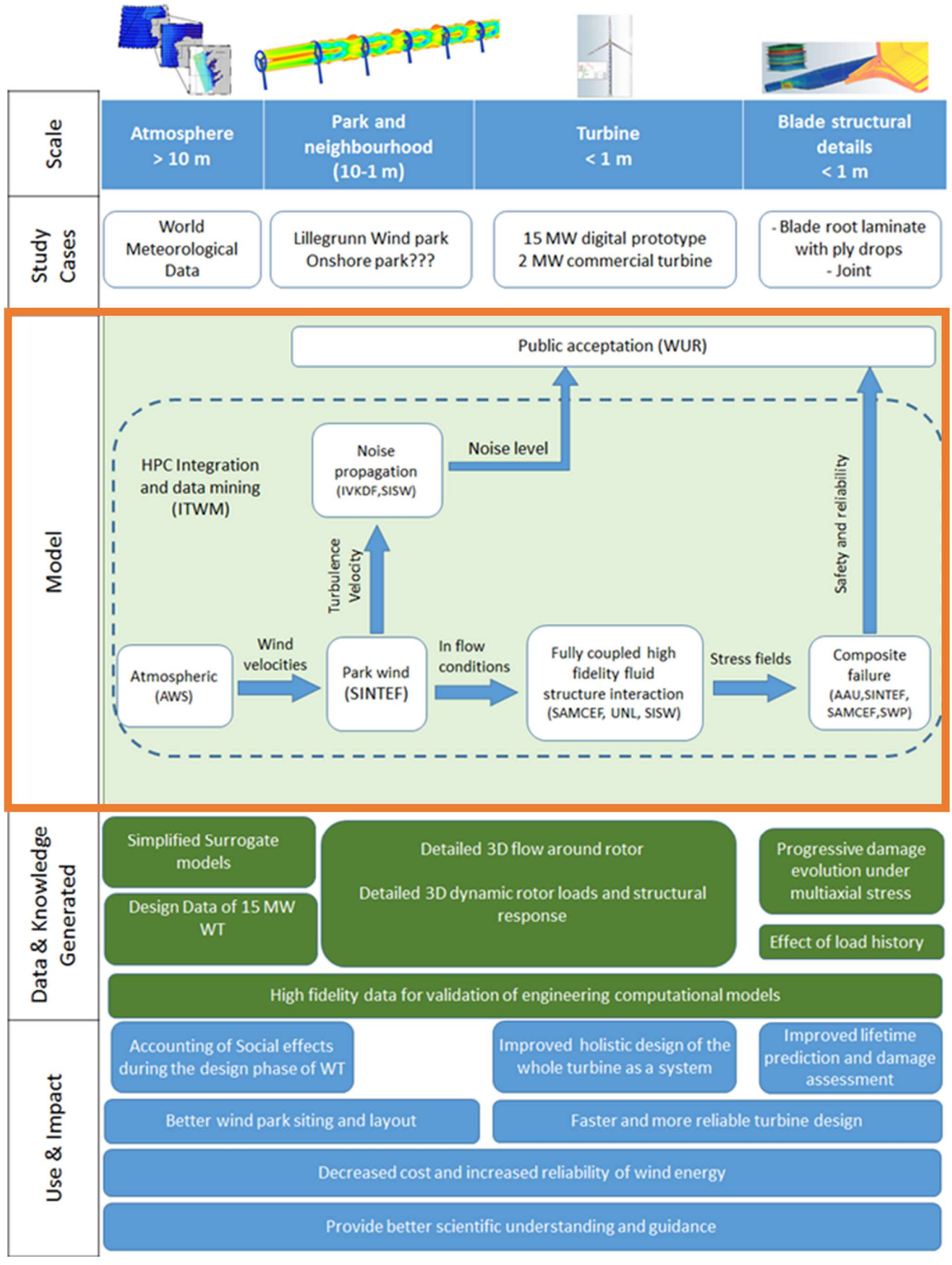

Figure 1: Design of Upwards simulation framework.

2. Study cases

The following case studies utilize the integrated simulation framework (as described in D6.3) to perform multiscale and multi physics studies of wind turbines and parks. The conducted data analytics provide deeper insight into complex coupled phenomena of wind energy engineering.

All study cases were conducted by using simulators within the integrated simulation framework (see Figure 1). The cases to be studied are:

Study Case 1: The effect of layout of turbines in offshore and onshore parks on wake, turbulence, productivity and turbine fatigue.

Study Case 2: The effect of size and position of onshore turbines on noise levels in the neighborhood.

Study Case 3: The influence of slender design of large blades (15 MW) on wind structure interaction, non-linear bending, buckling and complex structural stresses promoting structural damage.

Onshore case:

We base our analytics of onshore wind parks on the Høg-Jæren Wind Farm (see Figure 2)[4] in southern Norway. This wind farm contains 32 wind turbines with a total capacity of 73 MW and an annual production of 230 GWh.

Figure 2: Høg-Jæren Wind Farm

Offshore case:

Similar analytics regarding an offshore wind park were conducted using the Lillgrund (see Figure 3)[5] wind farm in the strait between southern Sweden and Denmark as reference. This Swedish wind farm contains 48 wind turbines with a total capacity of 110 MW.

Figure 3: Lillgrund Wind Farm

2.1. Study Case 1: Onshore park analytics

In this study case we investigate effects of wind turbines wakes and atmospheric turbulence within wind farms by using data-based analytics. The goal is to get useful insights into how these effects influence the productivity and stress of individual wind turbines.

[4] https://www.vindenergi.no/projects/hog-jaeren

[5] https://powerplants.vattenfall.com/lillgrund/

Onshore case: Høg-Jæren

Following the workflow of the integrated simulation system, we used the Weather Research and Forecast system (WRF) that has been extended in Work Package 2 to simulate atmospheric conditions covering wind direction and wind speed in this geo location:

latitude: 58.6442

longitude: 5.73794

height: 80m

We focused on two major wind conditions, and selected December 30th, 2017 to simulate wind coming from the southeast direction, and June 12th, 2018 to simulate wind coming from the northwest direction.

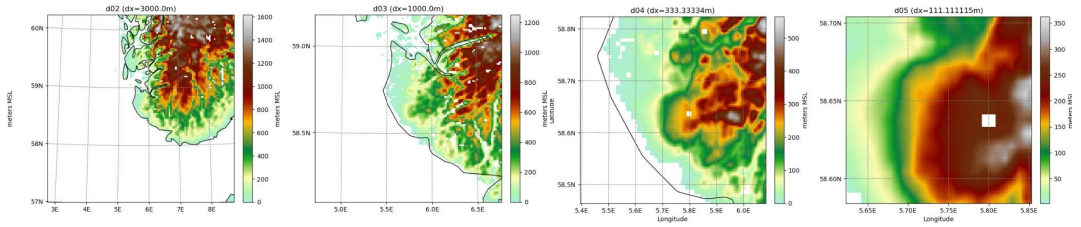

Figure 4: Terrain information on different height and detail levels

The meso scale weather simulation is capable of simulating conditions on different height levels (see Figure 4). We decided to simulate wind conditions at the height of 80m which is the turbine hub height for both offshore (Lillgrund) and onshore park (Høg Jæren).

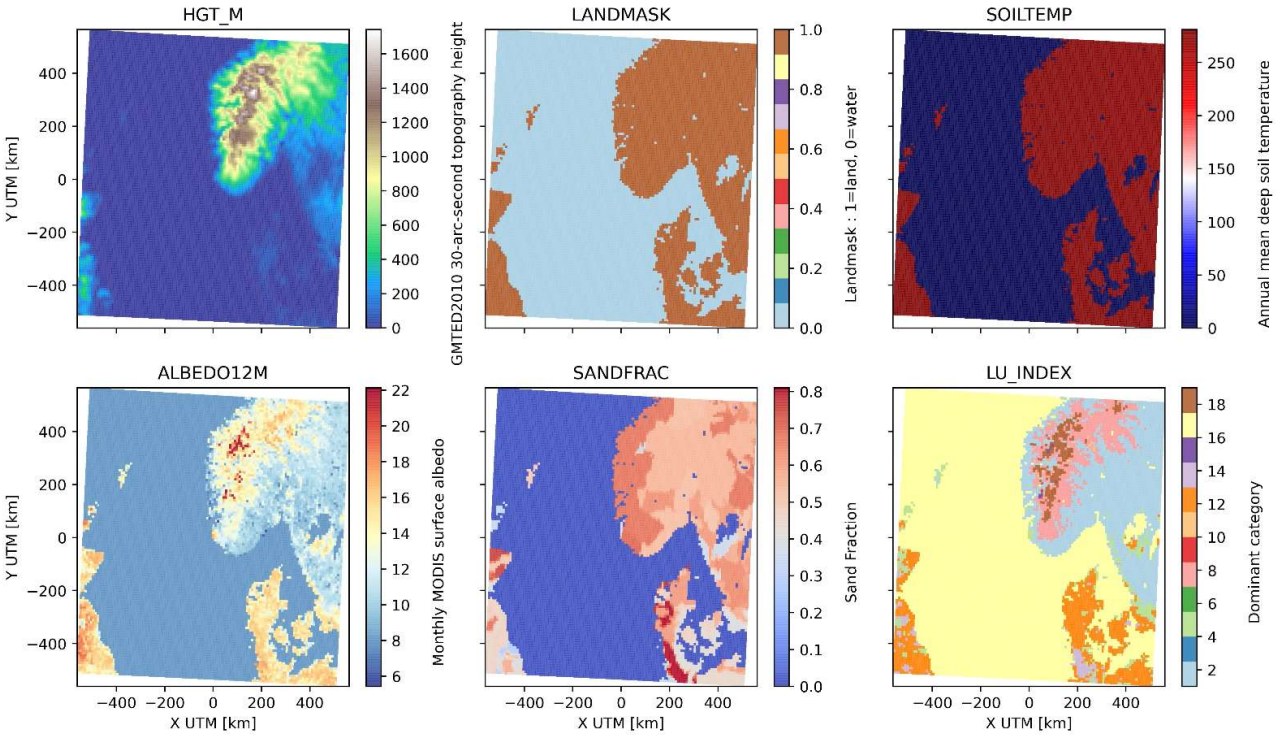

Figure 5: Terrain information on weather influencing variables

Wind conditions strongly depend on terrain and soil types. WRF is capable of using the geo information required to simulate turbulences at the Høg-Jæren location.

The simulation of turbulent flow fields in the scope of the wind farm was performed by using the OpenFoam system that has been extended in Work Package 2 within the integrated simulation

platform. We setup the Høg-Jæren park conditions to a subset of 9 turbines. The left image in Figure 6 depicts these 9 turbines on a map from Open Street Map, within the surrounding context.

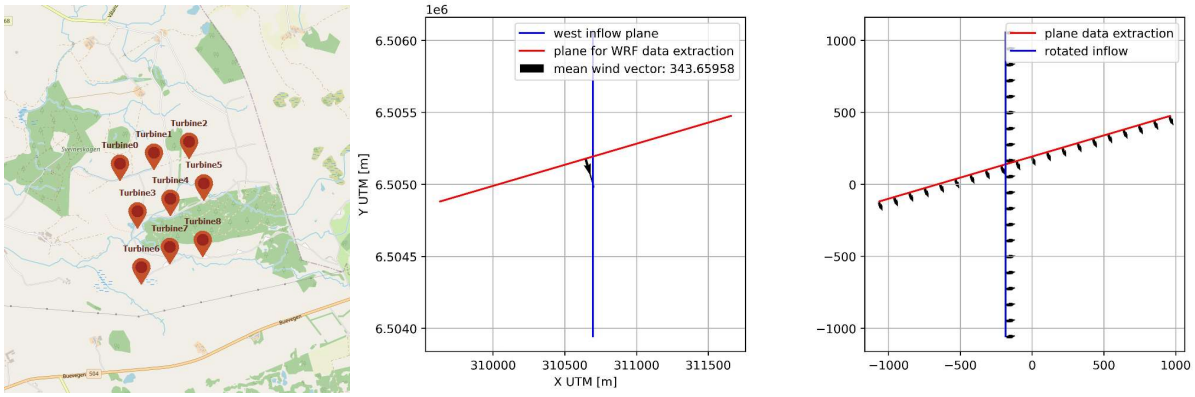

Figure 6: (Left) Subset of 9 turbines of the Høg-Jæren Wind Farm, (center) northeast wind direction, (right) transformation and rotation of WRF inlet surface to OpenFoam coordinates

We simulated the flow fields using an inlet surface that was extracted from the simulation output of WRF. Due to existing restrictions in the OpenFoam coordinate system, we had to convert the inlet fields from WRF to OpenFoam by rotation and coordinate conversion. The center and right chart in Figure 6 show details on how we translated the coordinate system and rotated the inlet surface.

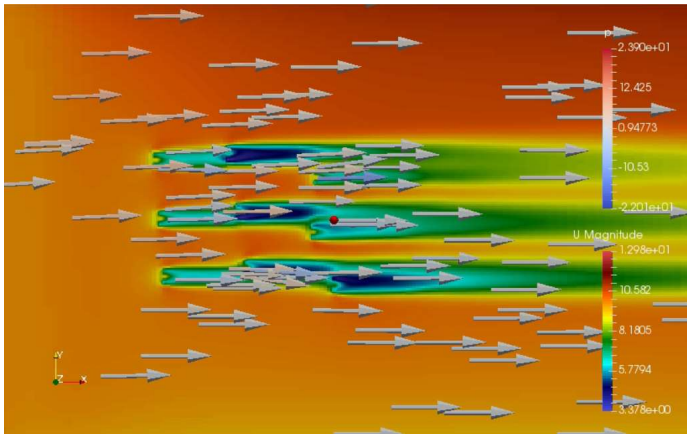

Figure 7: Simulated Flow fields with wind farm for northeast wind direction

Finally, Figure 7 shows how OpenFoam simulates the flow fields that emerged within the windfarm with a wind direction from northeast. Arrows denote major wind directions. The velocity contour plots indicate wind velocity. Here, the influence of wind direction and turbine positions on wake can easly be observed, as the downstream turbines in the second and third columns are highly influenced by the wakes emanating from the upstream turbine. This reduction in velocity causes reduction in the power production.

In this study case, we investigated these influences of the wake on wind turbines within wind farms under different yaw configurations. The yaw control system of wind turbines is responsible for the orientation of the wind turbine rotor towards the wind and in normal operation we assume that yaw misalignment is zero. However, we assume that wind turbines are equipped with an active yaw control system, such that the orientation of the rotor can be controlled towards a range of wind turbine shaft angles. Figure 8 shows on the left side an OpenFoam convention that a yaw of 270° defines an orthogonal angle in between the rotor and the wind velocity vector U_{wind}. Usually, one uses the term yaw misalignment to indicate a yaw angle different from 270°. A yaw angle of 270° corresponds

to a yaw misalignment of 0° while a yaw angle of 260° corresponds to a yaw misalignment of -10°. We will use the yaw misalignment in the following analysis.

We defined a wind farm as an array of wind turbines. Following this representation, we used the yaw misalignment of the first column of the array of wind turbines as input parameter. We investigated yaw misalignments in the range of +/- 30°. Turbines, that are located in a line with respect to the wind direction are called a row/line of turbines. In Figure 10 the setup of the turbines can be seen. In the northwest case for example the yaw angles of turbines 0, 1 and 2 were varied and the effect on the other turbines was analyzed. We especially concentrated on the effect that the change of the yaw misalignment has on a row of turbines (e.g., the effect of the yaw misalignment of turbine 0 on turbines 3 and 6 in the northwest case).

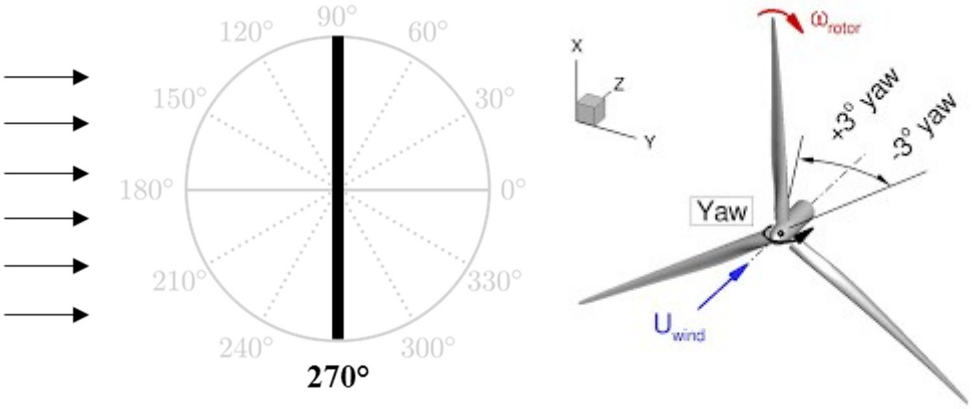

Figure 8: Yaw control system

For each operation point that is defined by a yaw angle value, we started a park simulation based on the inflow wind conditions from WRF. Figure 9 contains a top-down view and a front view of a wind farm. It shows mean wind velocity fields of three of such simulations in which the first column of wind turbines was configured with yaw misalignments of 0, 25° and –30° (which correspond to yaw angles of 270°, 295° and 240°).

The wake of the first column of turbines turns right for a positive yaw misalignment. It turns left when the yaw misalignment is negative. This effect is analysed in the succeeding case study, to see if the yaw configuration can be utilized to increase the performance of a wind farm in total.

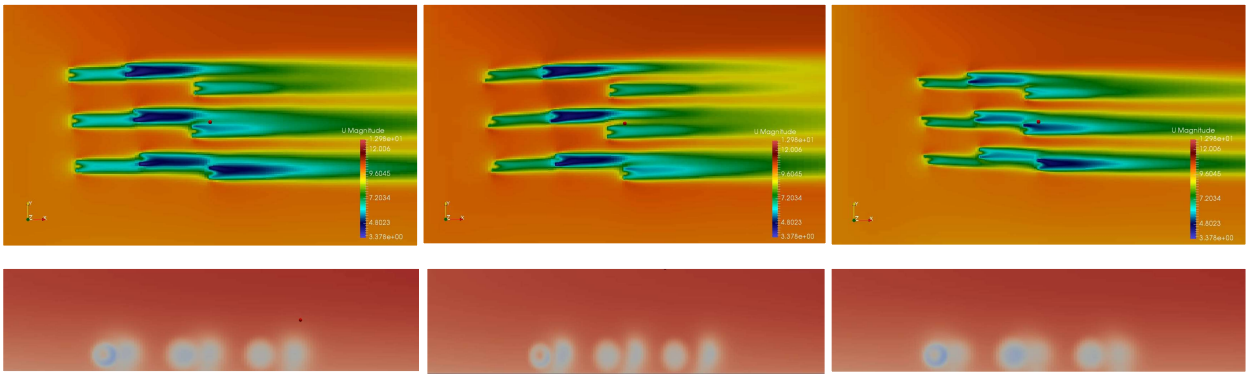

Figure 9: Flow conditions of the Høg-Jæren park for three yaw misalignments. Left: 0° / Center: 25° / Right: -30°

A modification of the yaw misalignment changes the resulting flow fields and wake situation within the wind park significantly. Within the setup of -30°, the wake after the first column decreases in width and intensity. This leads to an increase of approaching wind velocity in the second column.

Whereas rotating the first column to 25° results in a decrease of wake in the third columns of wind turbines.

In this study case, we analyse the effect of modified yaw angles on the generated power at generator level and experienced stress at blade level.

In order to facilitate the interpretation and validation of analysis results, we developed a simplified wake model for wind farms and wind directions based on the OpenFoam coordinate system. Figure 10 shows two perspectives on the Høg-Jæren park, respectively. The vertical lines represents the rotors' yaw angle of each turbine. Here, all turbines are aligned equally with a yaw misalignment of 0°. The left chart represents a northwest wind direction. Here, the overlapping rectangles highlight wake or partial wake effects between wind turbines. In the northwest case, the second column consisting of Turbine 3, 4, and 5 face a partial wake situation. In the southesast case on the right, the third column of turbines 0, 1, and 2 face a partial wake situation.

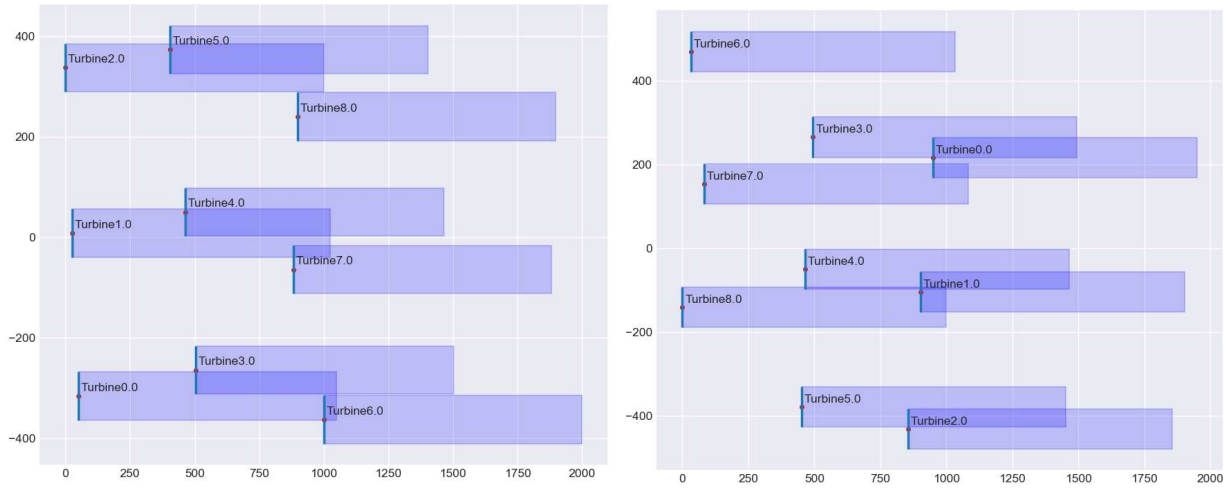

Figure 10: Simplified wake model of the Høg-Jæren windfarm. The left chart represents the northwest wind direction. The right chart represents the rotated park from southeast wind direction.

In the northwest case, we rotated the wind turbines of the first column, namely turbines 0, 1, and 2 in their yaw alignment. Within the southeast case, we decided to let the first column contain turbines 5, 6, 7, and 8, and let them rotate in yaw.

We conducted a parameter study on yaw and assigned the following yaw misalignments to park configurations:

Yaw misalignments:

[-30, -25, -20, -25, -10]

[-10, -9,…,-1, 0, 1,…,9, 10]

[10, 20, 25]

In the following analysis and interpretation of the case study, we will concentrate on the mean value and the variance of the produced power. The mean value is used to study the influence of the yaw angle on the produced power. In terms of variance s^2, we use the following mathematical formulation:

$$\bar{x} = \frac{1}{n}\sum_{i=1}^{n} x_i \quad s = \sqrt{\frac{1}{n-1}\sum_{i=1}^{n}(x_i - \bar{x})^2}$$

,

.

The physical interpretation is as follows: The standard deviation s (which is the square root of the variance) represents the amount of extraordinary changes in thrust which lead to the blade being pushed. These kind of impulses excite vibrations on blade level. Thus a large standard deviation/variance may hint at more stress being put on the blade which leads to fatigue.

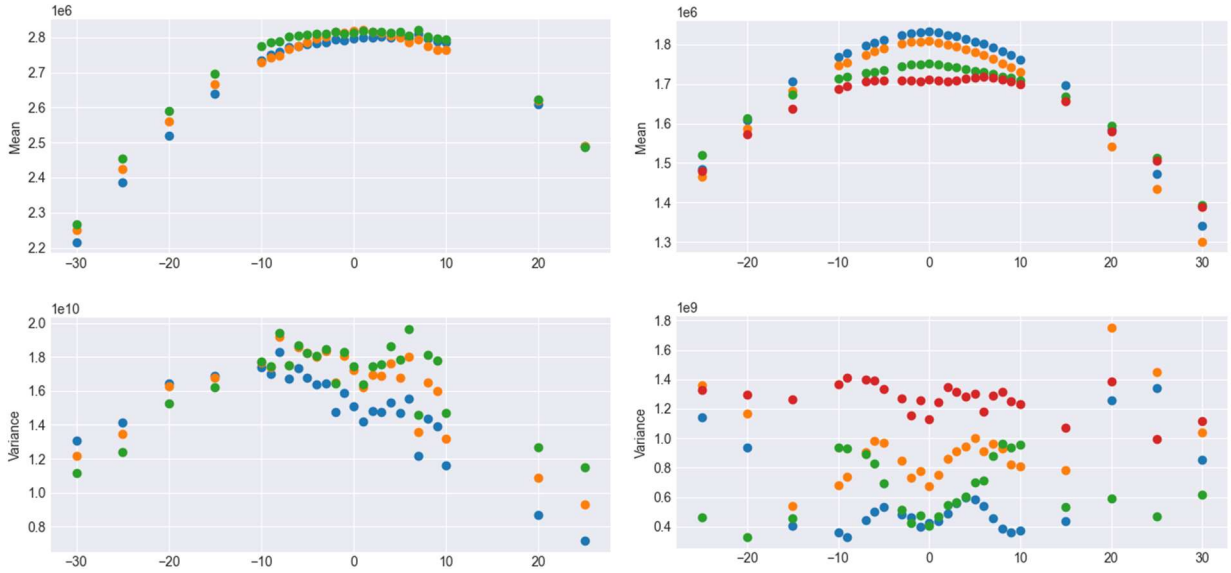

Figure 11: Power distribution (mean value and variance) of the first column of turbines. The yaw misalignment is on the abscissa.

First column analytics

Figure 11 shows the distribution of generated power by turbines of the first column. The northwest case is on the left while the southeast case is on the right. The upper charts represent mean power values for each yaw misalignment. The lower charts depict variances respectively. Each colour represents a single turbine. For the northwest wind direction on the left, colours denote:

Turbine0 (blue), Turbine1 (orange), Turbine2 (green).

For the southeast wind direction on the right, colours denote:

Turbine5 (blue), Turbine6 (orange), Turbine7 (green), Turbine8 (red).

The mean values resemble a gaussian curvature or a parabola. Differences between the turbines can be explained by differences in inlet wind velocity surface at the respective rotor positions. The peak exists in the area nearby a yaw misalignment of 0. The variance values show a saddle point at the same position. For the southeast wind direction, there is a local peak of the standard deviation at yaw misalignment of 20°, which is interesting. It might be explained by the fact that this configuration will increase turbulence effects.

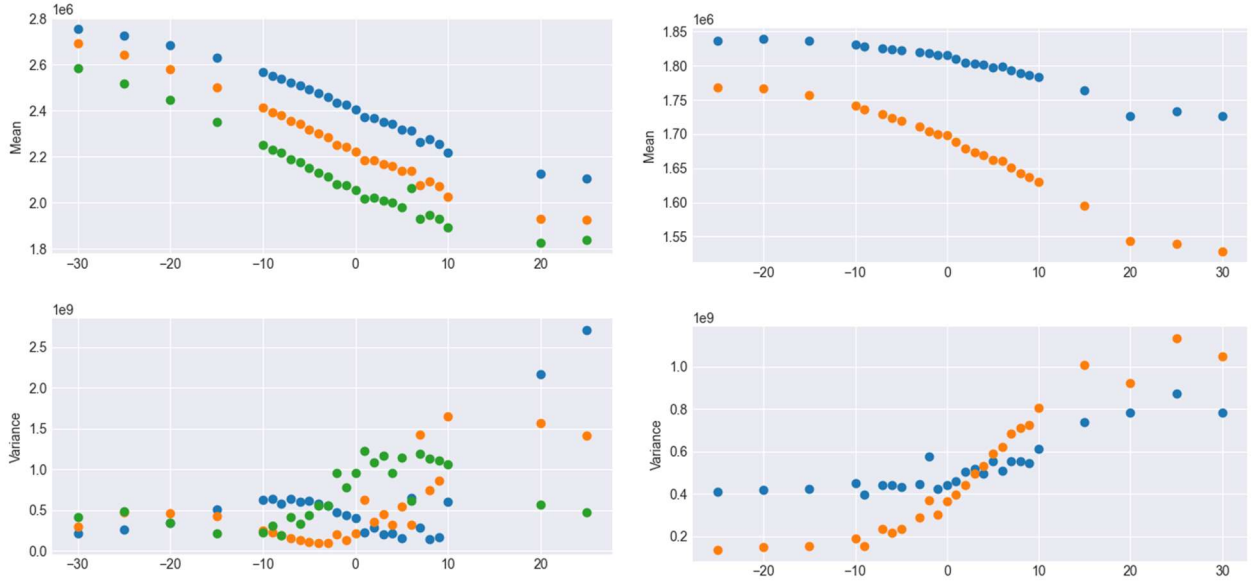

Figure 12: Power distribution (mean value and variance) of the second column of turbines. The yaw misalignment is on the abscissa.

Second column analytics

Figure 12 shows the generated power by turbines of the second column. The northwest case is displayed on the left and southeast case on the right. The upper charts represent mean power values of each yaw angle. The lower charts depict variances respectively. Each colour represents a single turbine. For the northwest wind direction on the left, colours denote:

- Turbine3 (blue),
- Turbine4 (orange),
- Turbine5 (green)

For the southeast wind direction on the right, colours denote:

- Turbine3 (blue),
- Turbine4 (orange)

The mean values follow a nearly linear path with decreasing gradient when increasing the yaw misalignment. Here, differences in height or gradient can be explained by differences in inlet wind velocity surface at the rotor position, which is in parts caused by a partial wake situation. Decreasing the yaw misalignment starting from 0 increases the resulting power of the second column of turbines significantly in the northwest case. The variance varies quite a bit for positive values of the yaw alignment. This effect probably shows a larger impact of partial wake situations. In the southeast case, the increase of power when decreasing the yaw misalignment is not as pronounced. Interesting to see is a non-constant gradient of mean values up to 20°. A reason might be an increase of partial wake effects. Turbine 3 remains more or less stable in standard deviation until 10°, increasing the yaw misalignment to a value higher than 10° also increases standard deviation. A reason is, that in these configurations the deflection of wake is so strong that it hits Turbine 3. Turbine 4 is positioned much closer to the wake of Turbine 8, hence the standard deviation increases constantly for positive yaw misalignments.

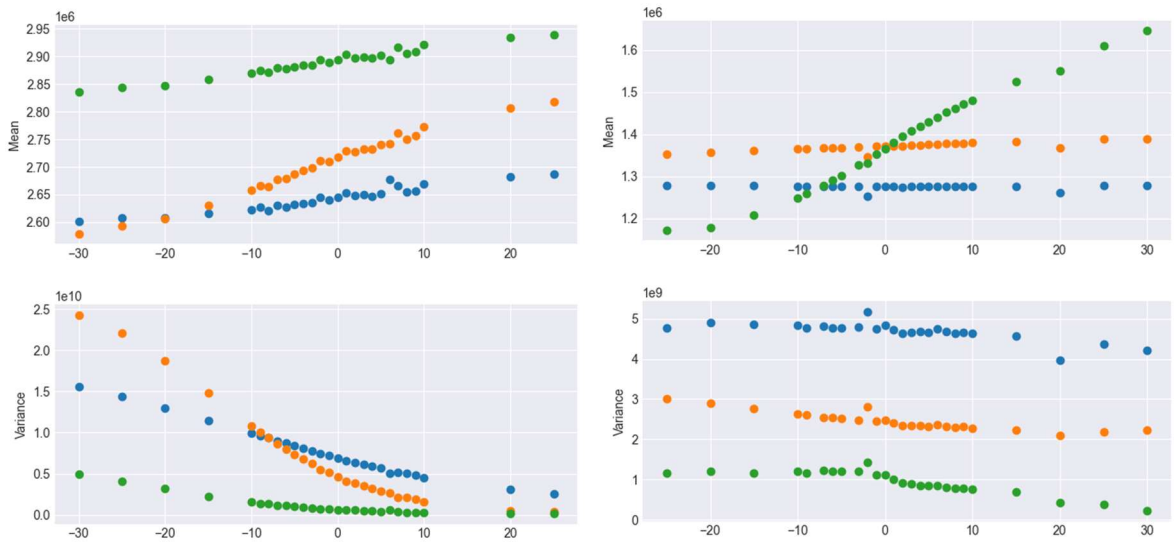

Figure 13: Power distribution (mean value and variance) of the third column of turbines. The yaw misalignment is on the abscissa.

Third column analytics

Figure 13 shows the generated power by turbines of the third column, in the northwest case on the left and in the southeast case on the right. The upper charts represent mean power values of each yaw angle. The lower charts depict variances, respectively. Each colour represents a single turbine. In the northwest wind direction on the left, colours denote:

- Turbine6 (blue),
- Turbine7 (orange),
- Turbine8 (green)

In the southeast wind direction on the right, colours denote:

- Turbine0 (blue),
- Turbine1 (orange),
- Turbine2 (green)

The mean values follow a nearly linear path similar to the study of column 2. However, the slope for the northwest case is positive here while the slope in the study of column 2 was negative. The reason for this is that the turbines in column 2 are on the right of the first turbines in the rows while the turbines of column three are on the left. Thus, the deflection of wake effects the columns in an opposing way. In addition, the slope in the southeast case is near zero except for Turbine 2 which is positioned in a partial wake.

From these findings, we can conclude that the control of the yaw of the turbines in the first column, affects the performance of suceeding turbine columns. Moreover the produced power decreases or stays constant when the standard deviation increases for the second and third columns. Thus, the goal of generating high amounts of power while simultaneously decreasing the stress put on the blades seems possible. This effect can be used in windfarm controllers that optimize the global performance of the wind park.

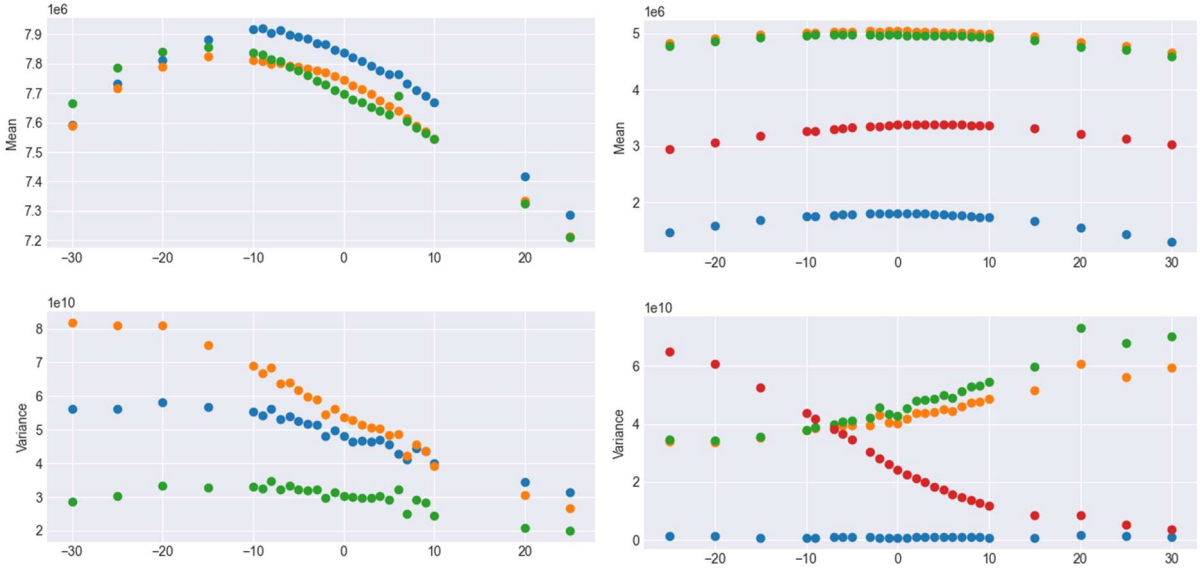

Figure 14: Aggregated power distribution (mean and variance) of rows of turbines. The yaw misalignment is on the abscissa.

Row analytics

Figure 14 shows the cumulative generated power by all turbines in one rows of the wind farm. Again, the northwest case is on the left while the southeast case is on the right. The upper charts represent the aggregated mean power values for each yaw misalignment. The lower charts depict variances, respectively. Each colour represents a single turbine. For the northwest wind direction on the left, colours denote:

- Row1 (blue, Turbines 0, 3, 6),
- Row2 (orange, Turbines 1, 4, 7),
- Row3 (green, Turbines 2, 5, 8)

For the southeast wind direction on the right, colours denote:

- Row1 (blue, Turbine 6),
- Row2 (orange, Turbines 7, 3, 0),
- Row3 (green, Turbines 8, 4, 1),
- Row4 (red, Turbines 5, 2)

Apparently, changing the yaw of the first turbines has more impact in the northwest case than in the southeast case. In the case where the wind comes from northwest, the optimal yaw misalignment setting is near -10°. This can be explained by the fact that all turbines of the second column are positioned left behind the front turbines. This partial wake can be compensated by decreasing the yaw angle of the first turbines. In additional, it also reduces the variance significantly.

The southeast case shows a rather resistant bevaviour regarding a change of yaw angles. The optimal working mode remains at 0°. The number of turbines in each row is clearly distinguishable by observing the offset. An interesting effect can be observed in the variance of Row4. Here, Turbine 2 is positioned parially behind Turbine 5 resulting in a partial wake situation. Thus, an increase of yaw misalignment reduces the variance since the wake is moved away from Turbine 2.

We conclude that row based yaw control influences the produced power of turbines significantly.

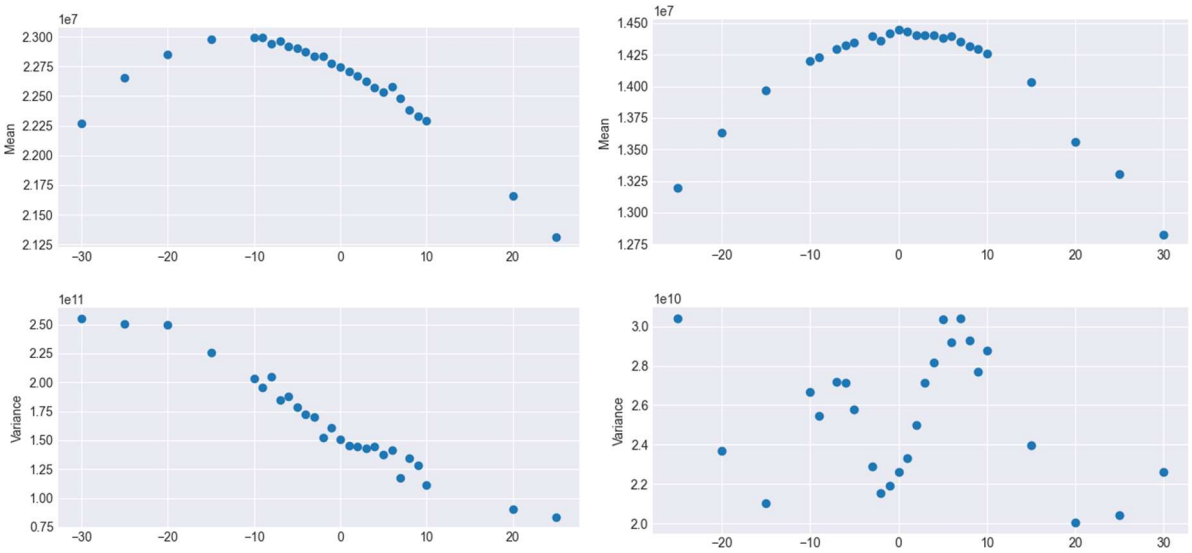

Figure 15: Aggregated power distribution (mean and variance) of a park. The yaw misalignment is on the abscissa.

Park analytics

Figure 15 shows the cumulative generated power by all turbines in the wind farm. Again, the northwest case is on the left while the southeast case is on the right. The upper charts represent the aggregated mean power values for each yaw misalignment. The lower charts depict the respective variances.

Similar to the row analytics, the northwest case shows an optimal yaw misalignment near -10°. The southeast case is at its optimum at 0°. The difference, when compared to the row analytics is that in park analytics the effects of yaw on the variance can not be interpreded separately for each turbine/row.

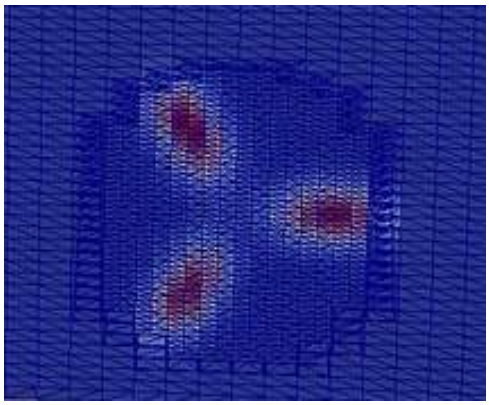

a) body force distribution

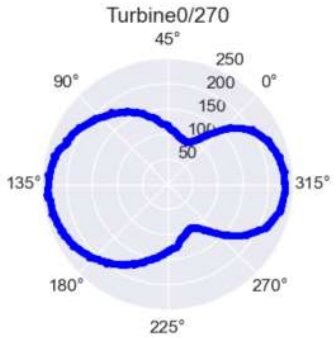

b) accumulated body force distribution

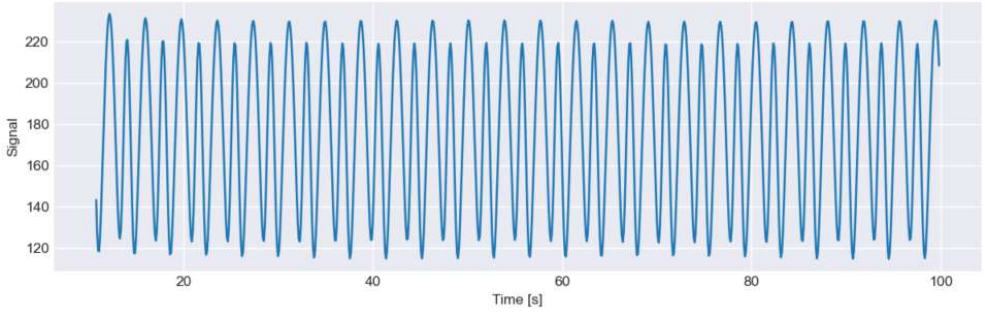

c) accumulated body force distribution over time

Figure 16: Body force distributions

Stress analysis on body force distributions

We calculated the experienced stress for each blade by summing up all body force values that are distributed along the blade. This calculation is performed for each snapshot. Finally, we observe the dynamics of these accumulated body force values with respect to time and rotation. If, during a rotation, a blade faces asymmetric differences of these body force values, we consider these events as being part of a stress cycle.

Extracted from an OpenFoam simulation, Figure 16.a shows a body force distribution along an actuator line model of a wind turbine. Red colored mesh elements denote lift or drag forces on a blade. It can be seen, that at the tips of the blades, the OpenFoam creates mesh-based fragments of this distribution. We address this issue by adding a Moving Average filter on the time series of accumulated body forces per snapshot (Figure 16.b and c).

Figure 17 present, for the northwestern wind direction, the radial body force distributions of the first columns of turbines of the Hogjearen windfarm along different yaw angles. These turbines face a free stream situation. It can be seen that with the change of the yaw misalignment the shape of the distribution is changing both in distance and rotation related to the rotor center and in extend. All turbines face the most symmetric radial distribution at yaw alignment of 0°.

When changing the yaw misalignment of the first column of turbines, the downstream shape changes in width and direction. Figure 9 shows flow conditions of the Høg-Jæren park for three yaw settings, left: 0°, center: 25° right: -30°. It can be seen that a reduced yaw misalignment rightwise turns the wake to the right (when looking upfront to the wind farm), a leftwise heightening of the yaw misalignment turns the wake to the left. Hence, a rightwise increase of the yaw misalignment turns wake away from Turbines 3,4,5 in the second column, but towards Turbines 6,7,8 in the third column. Heighting the yaw angle behaves vice verca. These effects are shown in the radial body force distributions of each turbine in Figures 18-20. Here, a partial wake situations appears as noise within the trajectory.

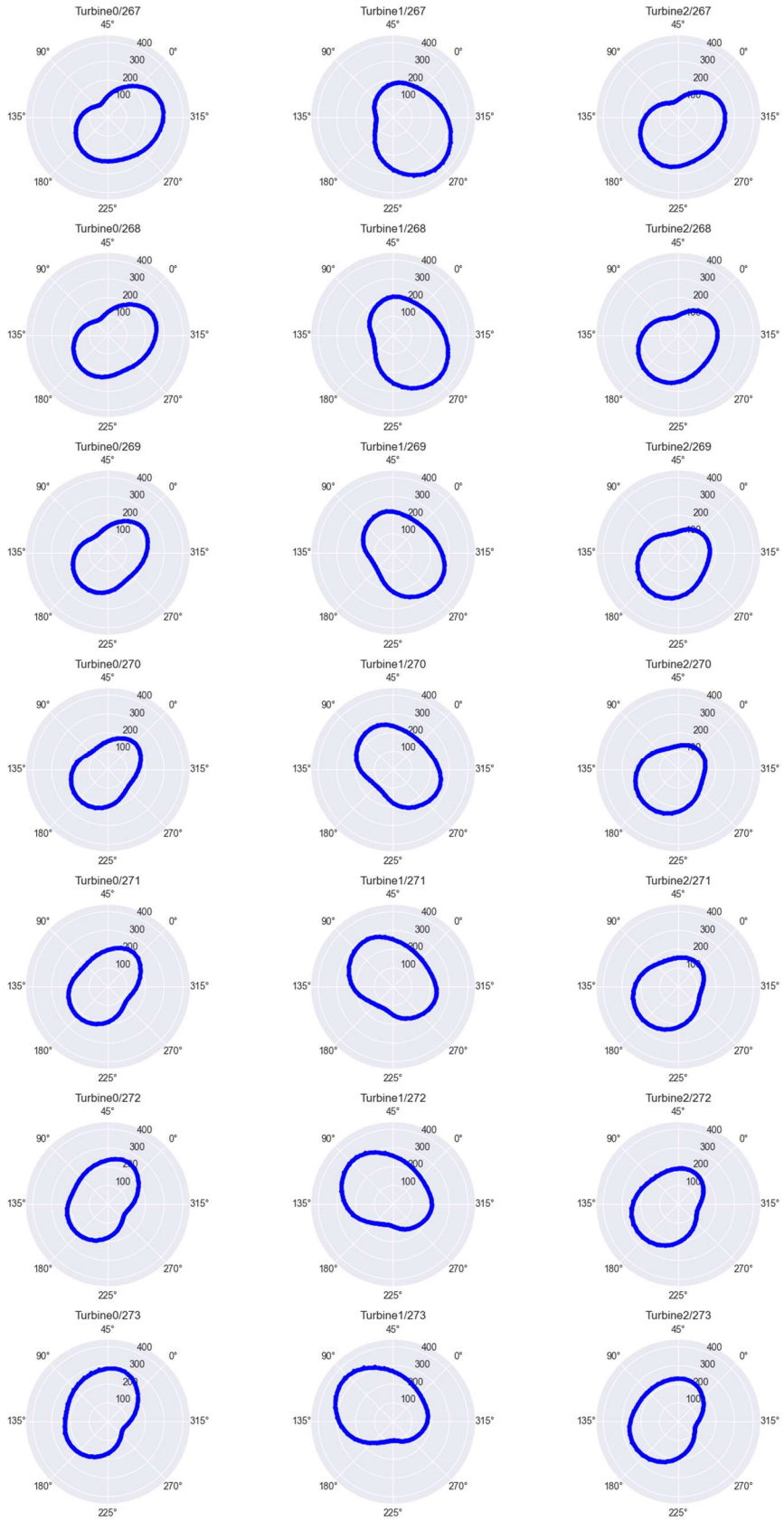

Figure 17: Aggregated body force stress cycles of first column turbines in Hogjaeren with a northwest wind condition (Turbine0, Turbine1, Turbine2)

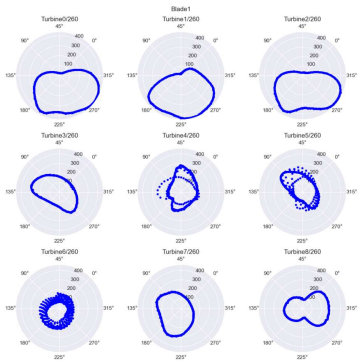

Figure 19: Radial body force distributions at wind=NW, yaw=-10

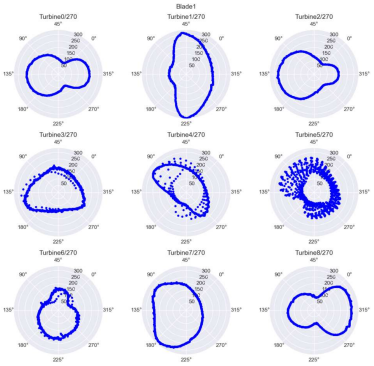

Figure 20: Radial body force distributions at wind=NW, yaw=0°

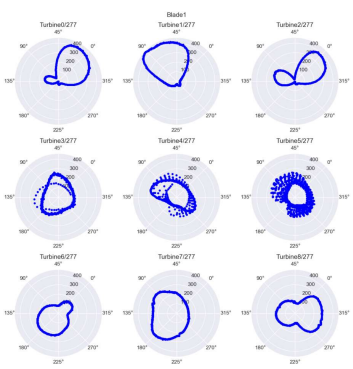

Figure 18: Radial body force distributions at wind=NW, yaw=+7°

The effect of partial wake situations on the body force distributions of turbines is figured out clearly, when visualizing the power spectral density of each turbine, as shown in Figures 21 and 22. Here the peaks represent the blade pass frequency and its harmonics. The amplitudes represent the amount of power of each frequency in the time series.

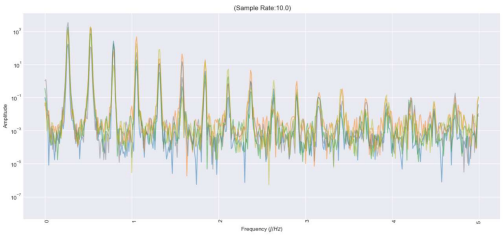

Figure 22: Power spectral density of body force distributions at wind=NW, yaw=270, Turbine0-2,7-8

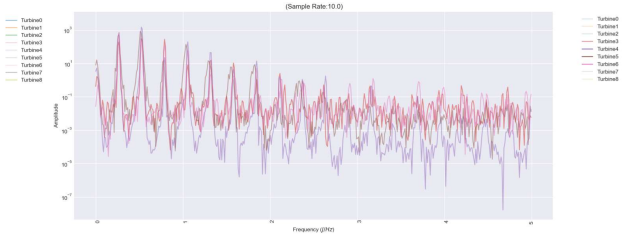

Figure 21: Power spectral density of body force distributions at wind=NW, yaw=270, Turbine3-6

Figure 21 contains the turbines in a free stream condition (Turbines 0-2, 7-8). Figure 22 contains the turbines in a partial wake situation (Turbines 3-6). Obviously, the wake induced noise causes disturbances of the blade pass frequencies.

Conclusion

In conclusion, the park analytics on Hog Jaeren revealed interesting findings in the simulated data:

1. Partial wake situations cause effects on reduced power, produced by those turbines within a partial wake.
2. Turbines within a partial wake show an unbalanced radial body force distribution on blades.
3. The unbalance is also visible as transient and noisy frequency spectrum of body forces.

These effects cause material stress. In general, partial wake situations can be improved by changing the yaw misalignment of freestream or front turbines. The fluid effects on material stress will be analyzed in next section.

2.2. Study Case 1: Onshore park analytics on fluid-structure interaction

Specification of simulation data required by FSI simulations

Fluid-structure interaction simulations require instantaneous field data (the three components of the velocity and turbulence fields) which must be provided by the simulations of the entire park. These data serve to fix the inlet boundary conditions at every time step.

The sampling plane should be located at a position between the analysed wind turbine (WT) and its predecessor. To avoid any virtual accelerations, the optimal distance upstream of the WT should be at least *5d*, being *d* the rotor diameter. However, this last requirement is slightly flexible to match the location of the WT in the park. Final distances from the sampling plane to the rotor should be communicated from the park simulations to this high-fidelity analysis to match both computational domains.

The wind information should be provided for a discretized vertical rectangular grid. The centre of this grid should match the nominal/initial location of the WT rotor centre and the height and width should be the same as the virtual wind tunnel built around the wind turbine.

The necessary wind flow information is the time history description of the 3D wind velocity vector, and the turbulent field parameters (kinetic turbulent energy and dissipation). For the BEM simulations, the turbulence fields are not used in the exchange algorithm. Instead, the turbulence accuracy will depend entirely on the spatial and temporal discretization of the provided wind data.

To improve the representativity of the wind turbulence on the rotor, the discretization is not uniform across the whole inlet plane. In the area roughly spanning *1.5d x 1.5d* around the rotor centre, the discretization should be finer, and the probes should be relatively well equispaced in width and height. The cloud of points over the entire inlet follows a structured mesh so that the finer discretization in the centre propagates above it, below it, and to the left and right sides.

The minimum grid spatial discretization in the central rotor-facing area is specified as:

- Maximum spacing in width and height between 2 consecutive probes = *0.2d*
- Probes roughly equally spaced in width and height

Data is communicated using files. In this context, from the wind farm simulation, a data file is built with data samples properly distributed at the relative location of the inlet patch of the selected wind turbine at the wind park.

The temporal discretization for the wind exchange should be specified as:

- Maximum time step between 2 consecutive history points = 0.02 s

CFD simulations for the isolated WT analysis are performed using the Simcenter STAR-CCM+ software. There, an *userlib* was developed to communicate the wind input at the inlet to the software. This *userlib* takes a series of input files with the description of the wind flow field for a particular time-sampling. Then, these tables are used to set the unsteady boundary condition. Spatial and temporal low order interpolations (nearest neighbour and linear neighbour respectively) are performed to project values from sampling locations to the cell centres that define the inlet patch at a given time. Similarly, the initial condition of the CFD simulation is supplied from the temporal data provided.

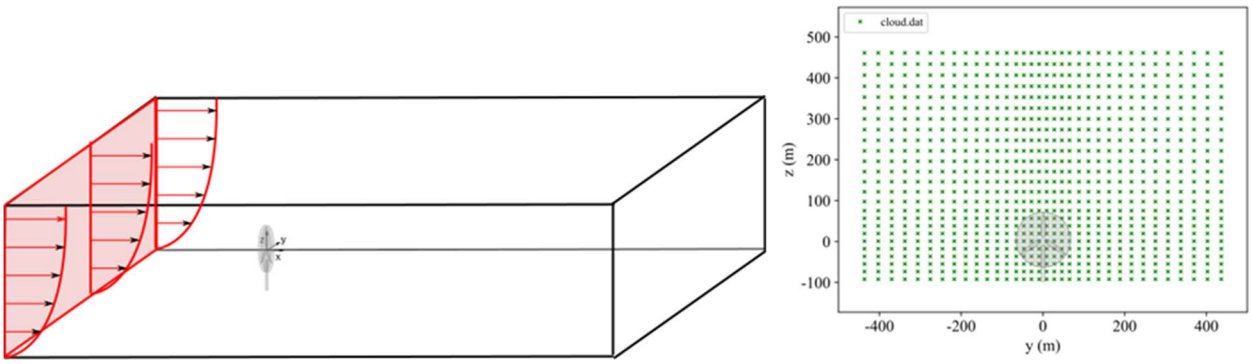

Figure 23: Example of the distribution of the sampling points. The distance from the centre of the rotor to the sides and to the top boundaries are 3xd.

Wind turbines number 1 and 4 of the Høg-Jæren wind farm are selected to perform the analysis.

Results for wind turbine 4

This wind turbine is located in the wake induced by wind turbines 0 (left), 1 (centre) and 2 (right). Figure below presents a snapshot of the incoming velocity field for WT 4, where the wake of the preceding wind turbines in the flow is noticeable. This flow pattern decreases the mean flow speed at the rotor height from 12 m/s (freestream) to approximately 7 m/s due to fact of being located exactly in the wake of the preceding wind turbine for these wind conditions.

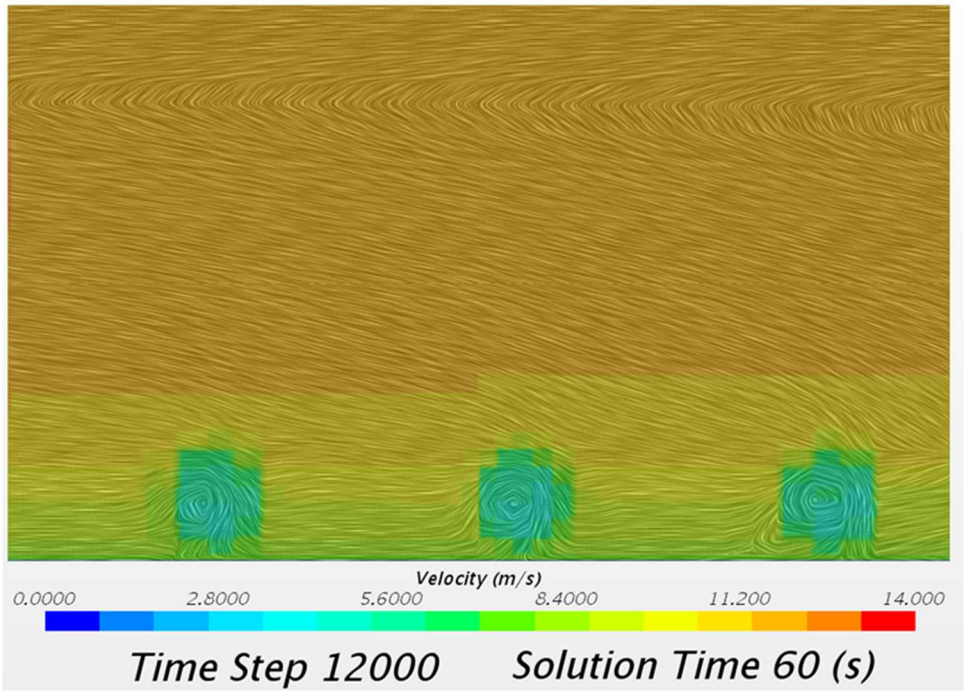

Figure 24: Snapshot of the inlet velocity field at time 60s (front view).

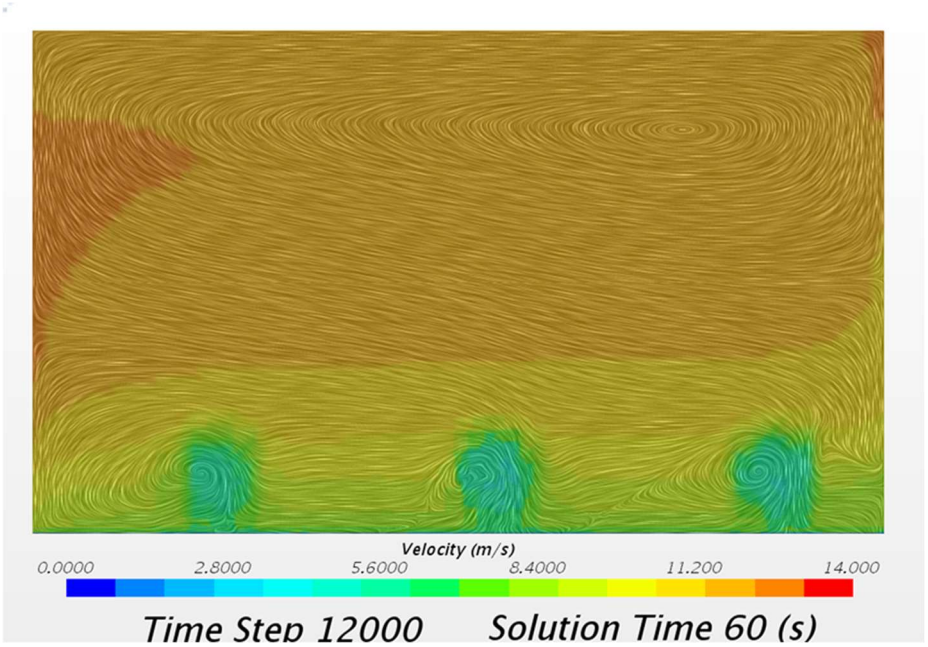

Figure 25: Snapshot of the velocity field located 150 m from the inlet at time 60 (front view).

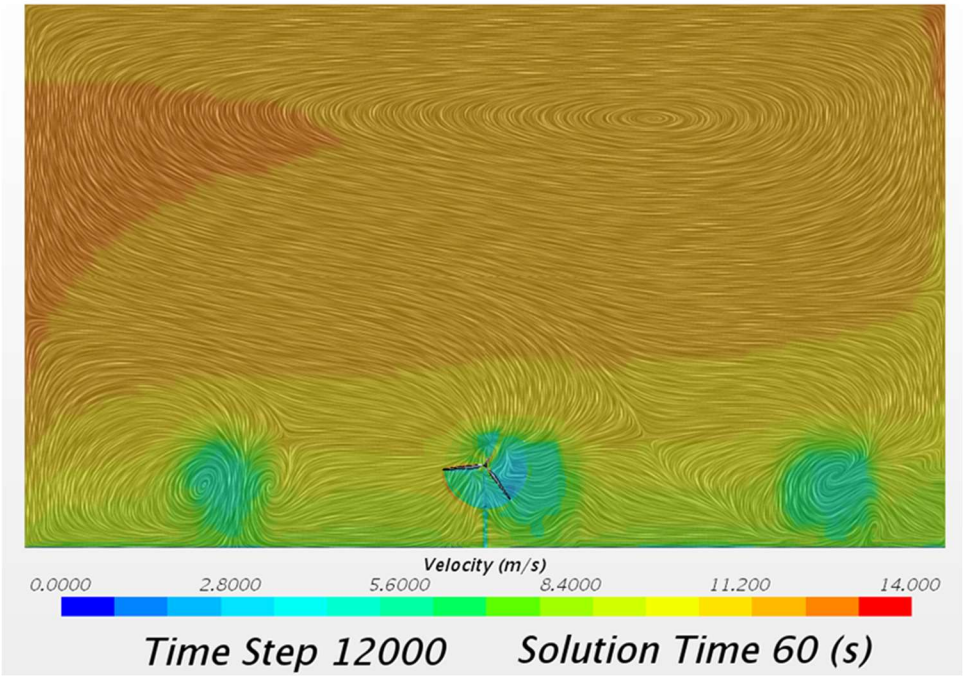

Figure 26: Snapshot of the velocity field located 300 m from the inlet at time 60 (front view).

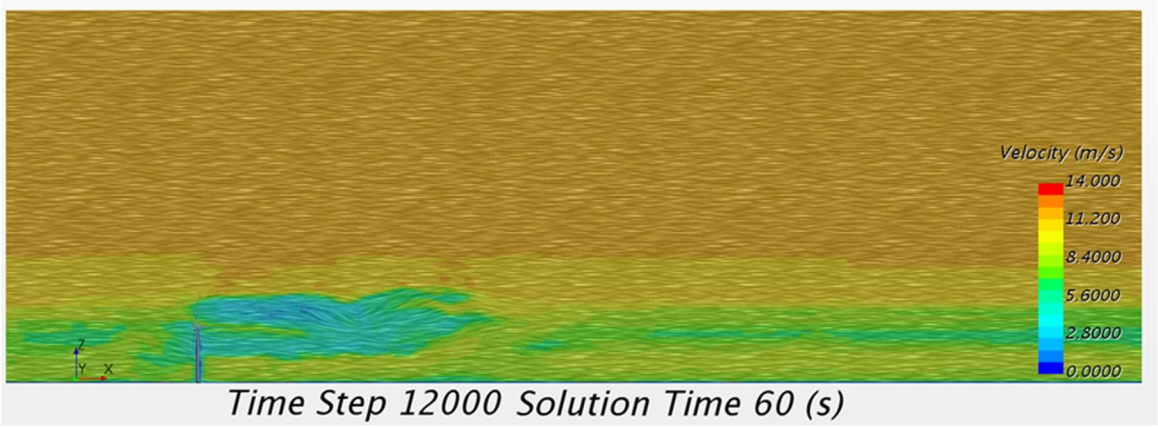

Figure 27 Snapshot of the velocity field at time 60s (lateral view).

The co-simulation evolves up to reaching 60 s of simulation time. The CFD simulation employs a finite volumes approach with second order discretization in space and first order in time to solve the URANS equations with the realizable k-epsilon turbulence model. The SCORE tool communicates the fluid forces over the blades to the mechatronic solver. Then, Simcenter Samcef Mecano returns the computed displacements to the fluid solver, which adapts the mesh to the new conditions. Since the time step should be small enough to guarantee convergence and accuracy of the fluid solver, only one coupling iteration per time step is needed. Figures 25-27 show the velocity field when interacting with the WT. Figures 28-30 show the behaviour of the wind incidence velocity near the WT.

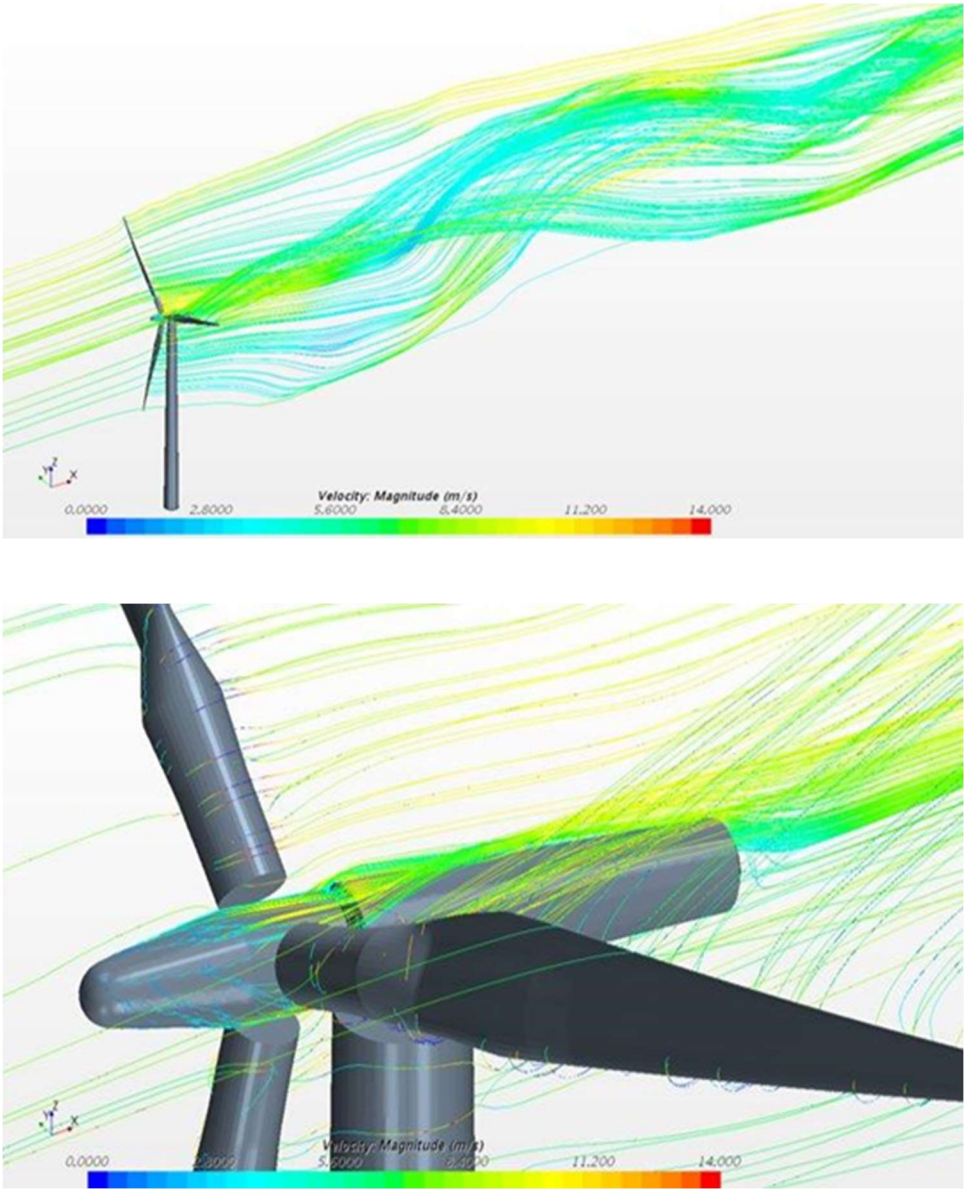

Figure 28: Snapshot of the streamlines at time 60s

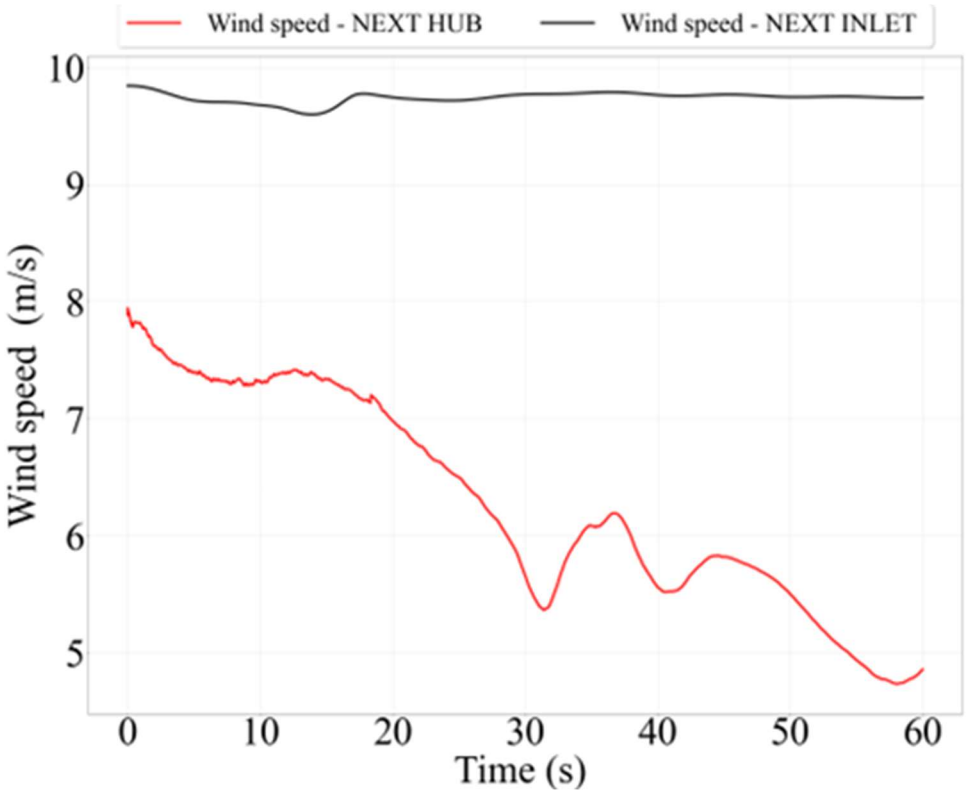

Figure 29: Wind speed at the inlet and next to the hub

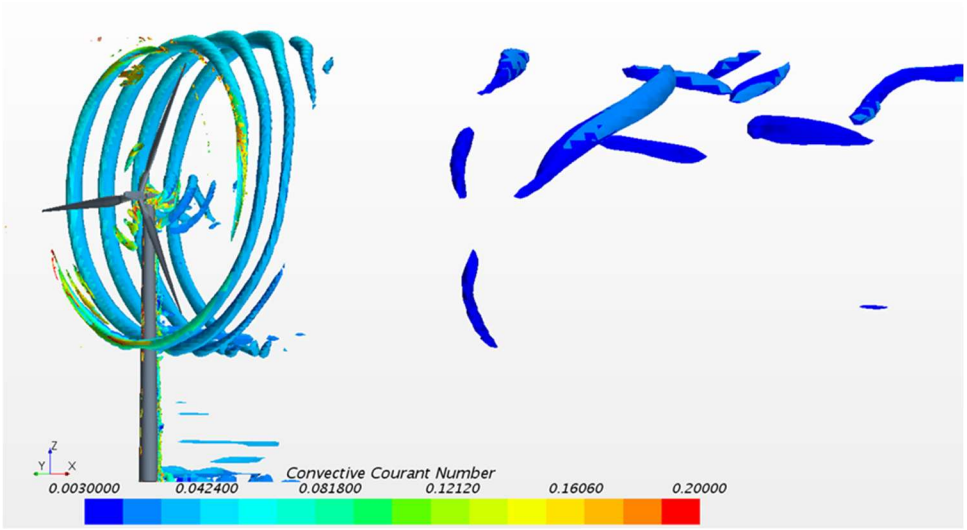

Figure 30: Turbulence patterns behind the wind turbine

The WT is initialized with the operative conditions (rotor speed) compatible with a freestream wind of 12 m/s. As the incident wind speed in the wake is lower, it is not enough to preserve that rotation speed. Under these conditions, the generated power is lower than the 2.3 MW expected, as shown in Figure 31

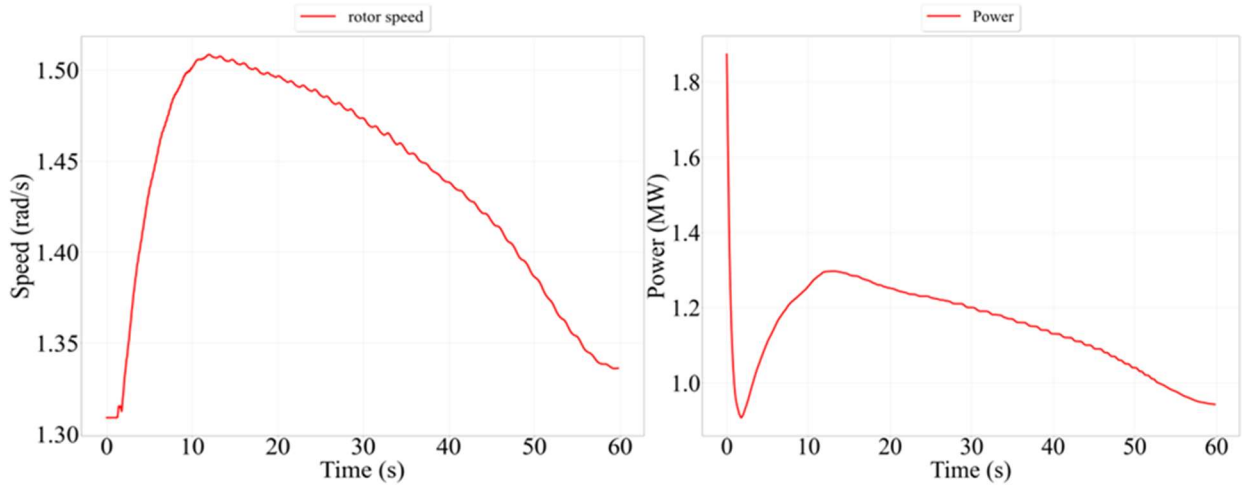

Figure 31: Rotor speed (left) and generated power (right).

Figure 32 shows that the control system decreases the blades' pitch down to the minimum limit. Nevertheless, it is not able to keep the desired operative conditions.

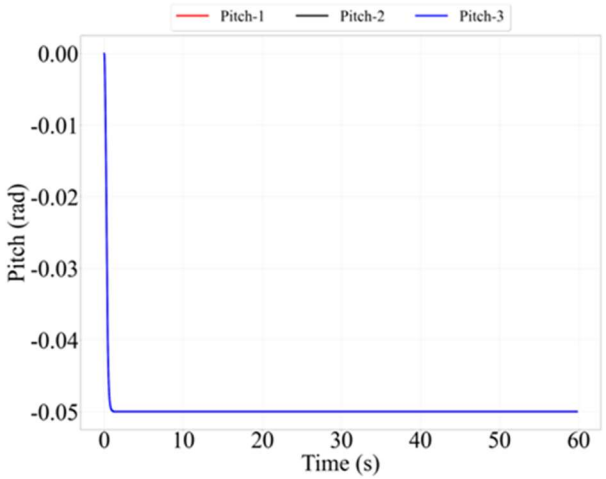

Figure 32: Blades pitch evolution.

Finally, Figure 33 presents the displacements of the blade tips. Due to the transient induced by the initial conditions, an overshooting is observed at the beginning. After that stage, the mean of the displacements varies according to the rotor speed. The amplitude of the displacement is almost constant at approximately 0.4 m. High-frequency patterns are noticeable when the blade tips reach the maximum displacement (when the blades are located at the maximum height).

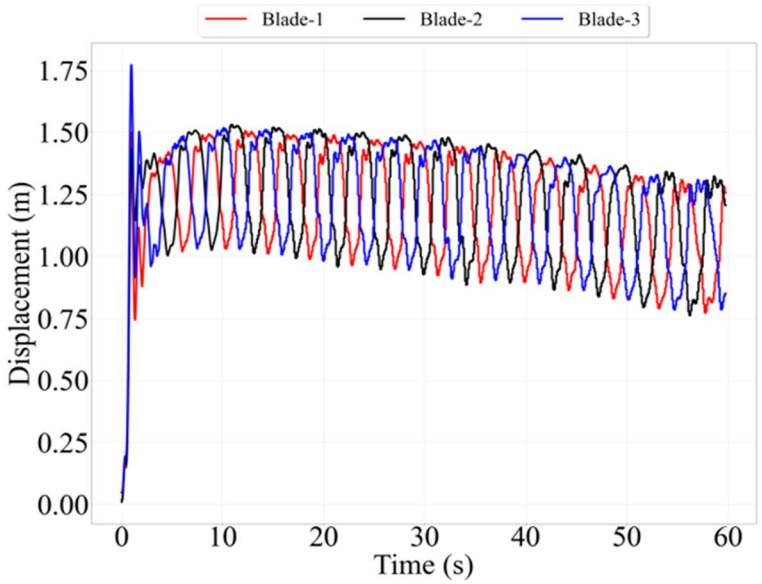

Figure 33: Blades tip displacements.

Results for wind turbine 1

In this case, the wind turbine is in the first row in the direction of the wind and the inlet velocity is not affected by any preceding WT. The mean inlet wind speed is 10.5 m/s.

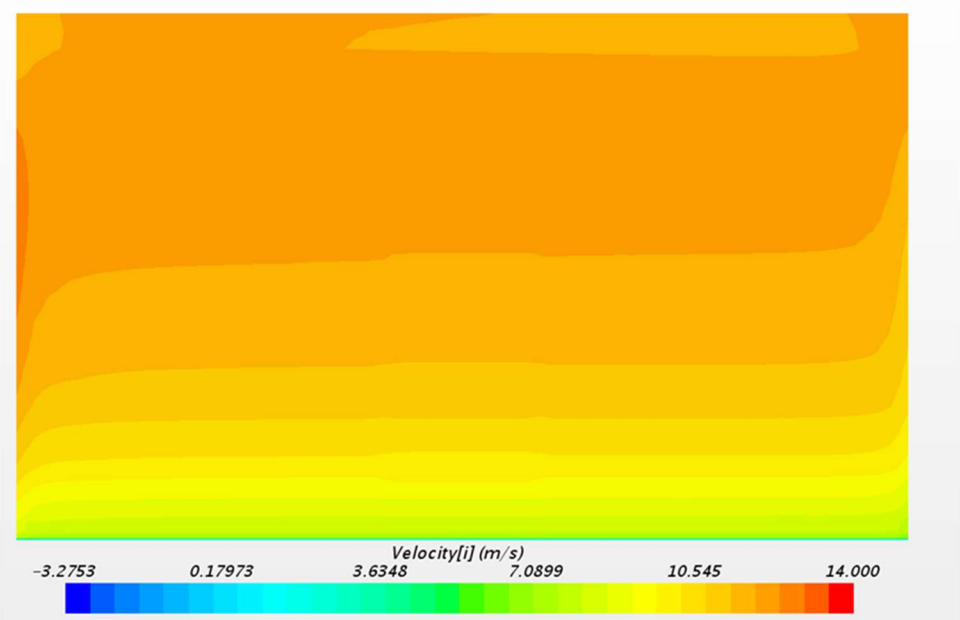

Figure 34: Snapshot of the velocity field at the inlet plane.

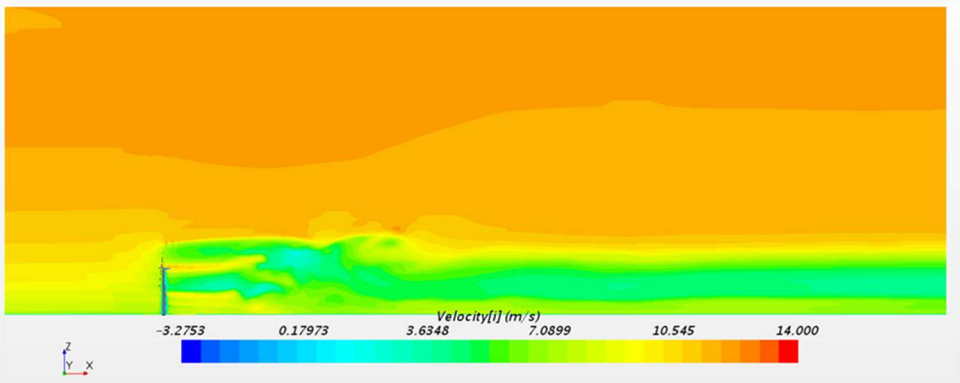

Figure 35: Snapshot of the velocity field (lateral view).

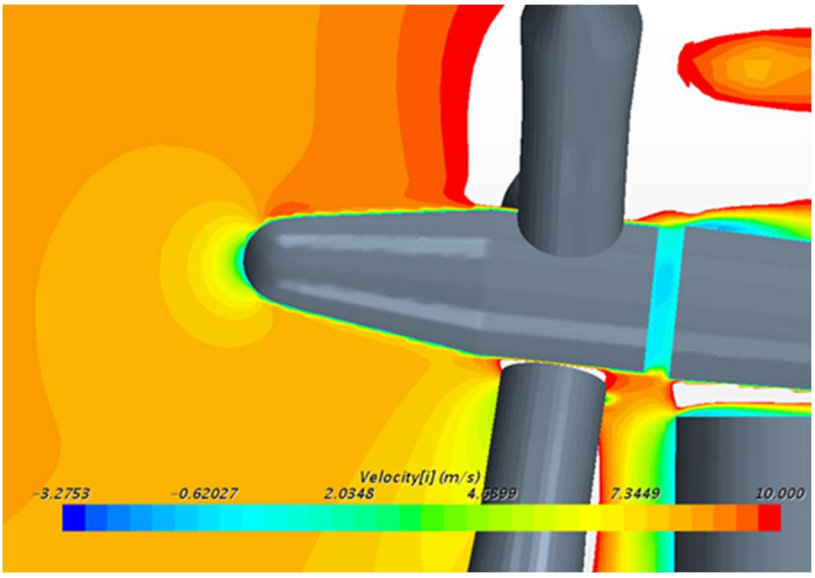

Figure 36: Sensor location next to the hub

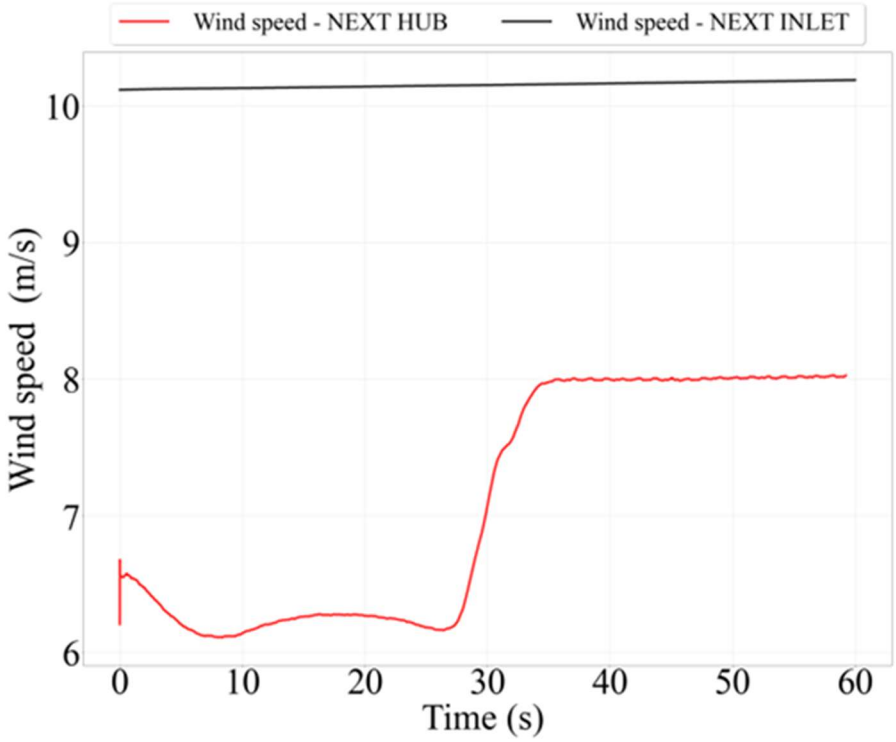

Figure 37: Wind speed at the inlet and near the hub.

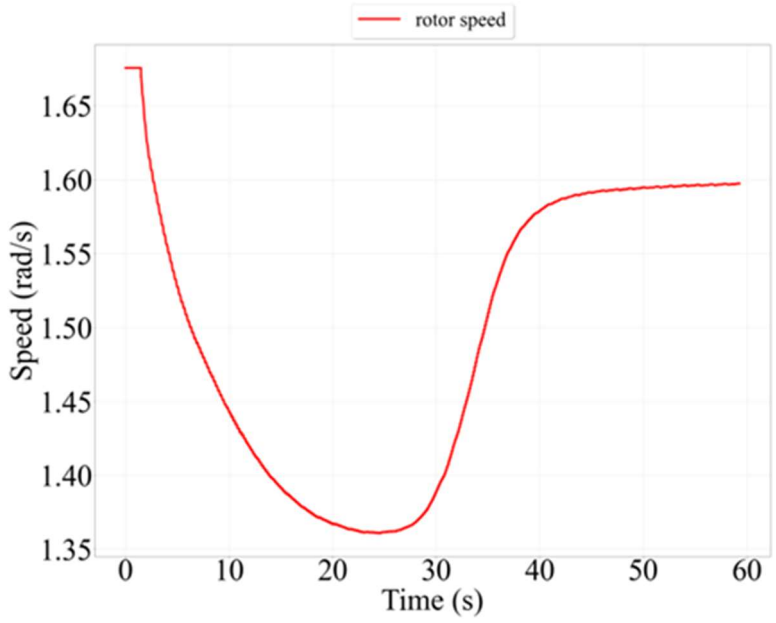

Figure 38: Rotor speed.

Figure 37-38 show the computed average rotor speed is 1.60 rad/s. This value can be compared to the nominal reference value of 1,57 rad/s.

Figure 39 shows the computed power is 1.7 MW and the torque is 0.012 MNm. These values correspond to nominal values.

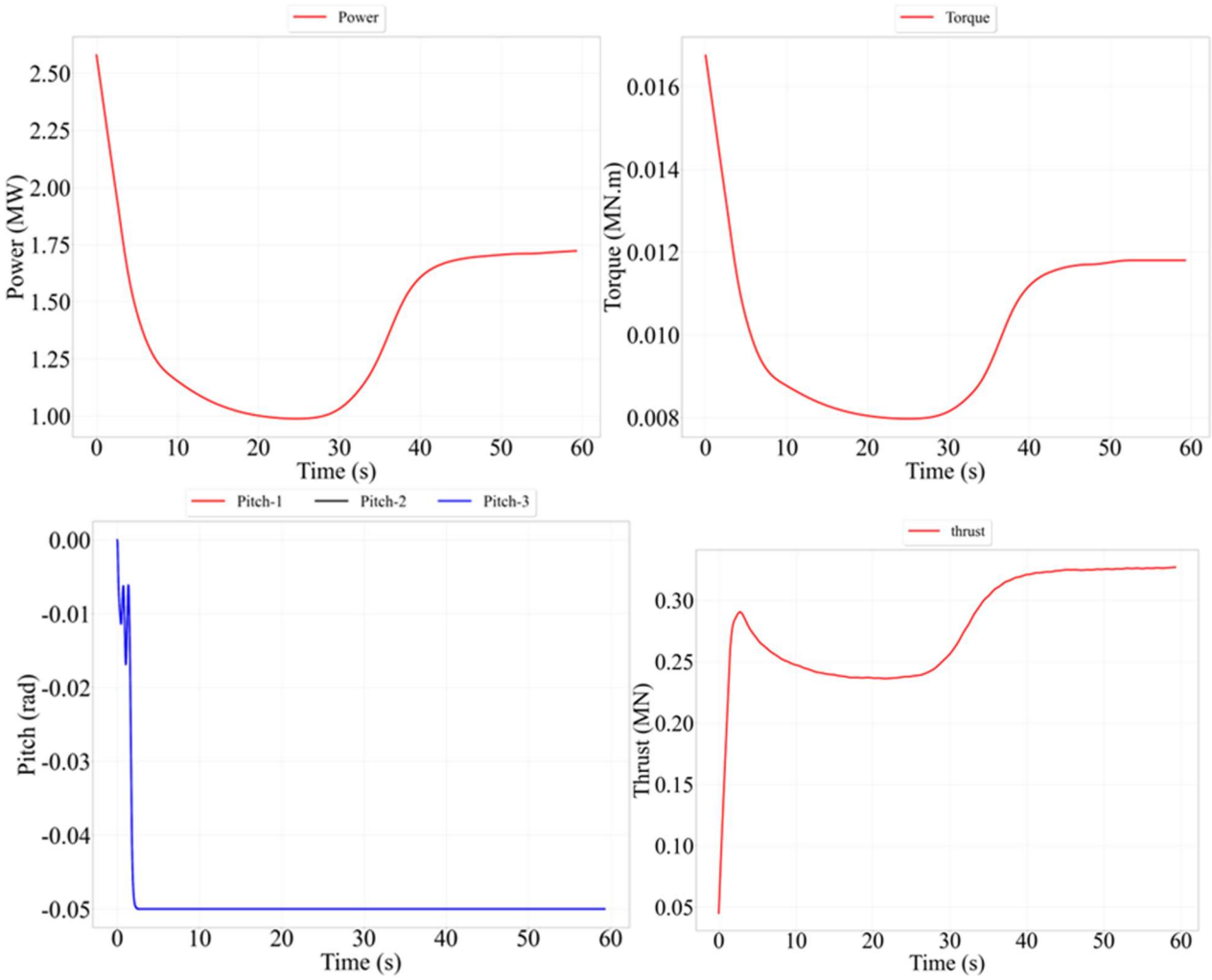

Figure 39: Generated power, torque, pitch, and thrust

The pitch angle is 0. This corresponds to the moment of maximum demand of the turbine. The thrust is 0.3 MN.

The maximum displacement at the blades tip is 1.5 m. A high frequency content is observed. When comparing these results with those obtained for Turbine 4 (operating in a significant partial wake) shown above, it can be seen that the blades of Turbine 1 experience higher mean deflections but significantly lower oscillations. This result was already detected using the BEM computations, with slightly different values. The high-fidelity CFD FSI seems to feature a higher frequency content which could be relevant in terms of blade fatigue loading (see Figure 40).

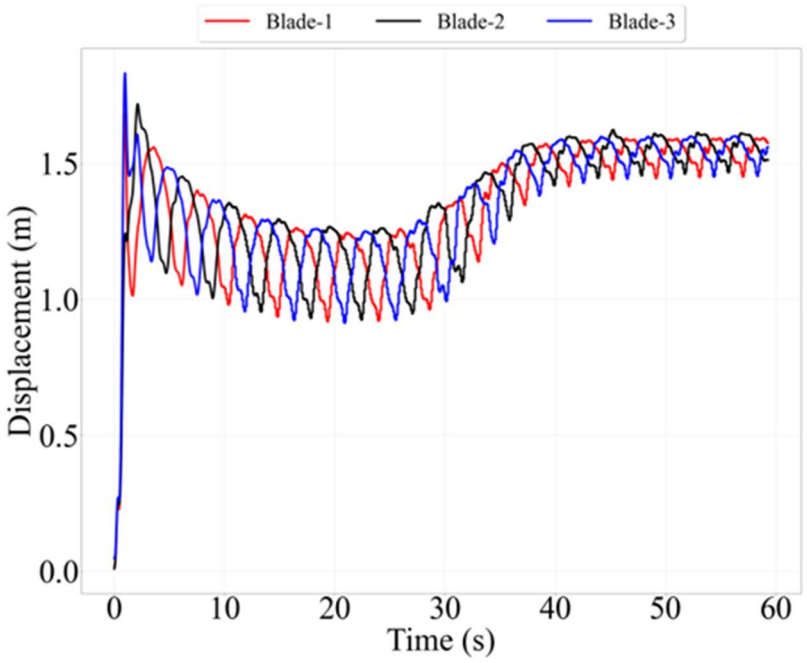

Figure 40: Tip displacement

Local Stress analysis on a composite blade

In D3.7, we presented the process to extract loads from the model of a full wind turbine considering fluid-structure-control interaction models developed in the scope of WP3, and to perform stress analysis on a detailed model of a sub-component of the whole system.

From the transient simulation of the wind turbine done either from BEM or FSI models. The global procedure to extract loads from the global mechanical model to a detailed 3D model of a place of interest along the blade is illustrated on Figure 41.

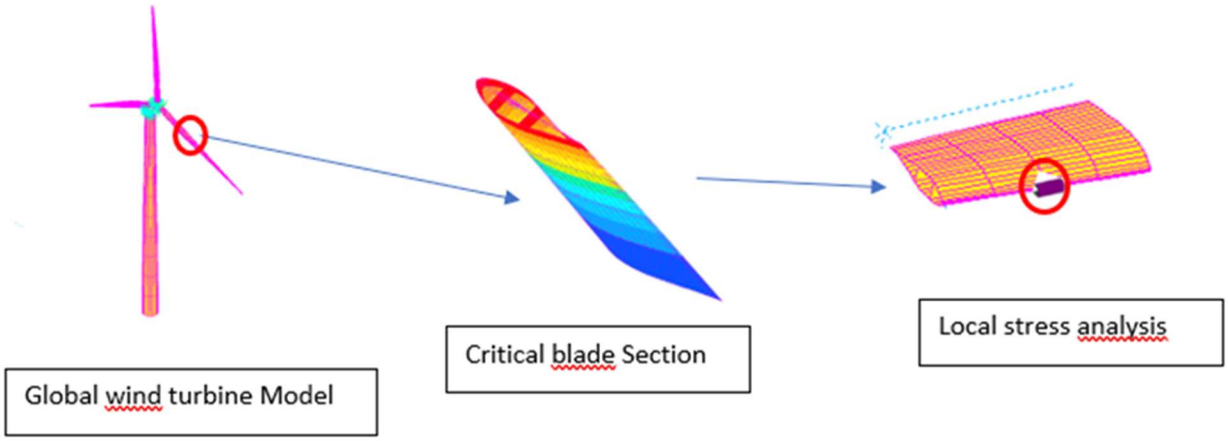

Figure 41: Process to perform stress analysis of a wind turbine component

The critical blade section is in the area where the chord is maximal. So, when we run the BNREL program to create the mechanical model, we selected two radius R1 and R2 that surrounded this section. Figure 42 shows the full blade, and the associated shell model that contains the critical section.

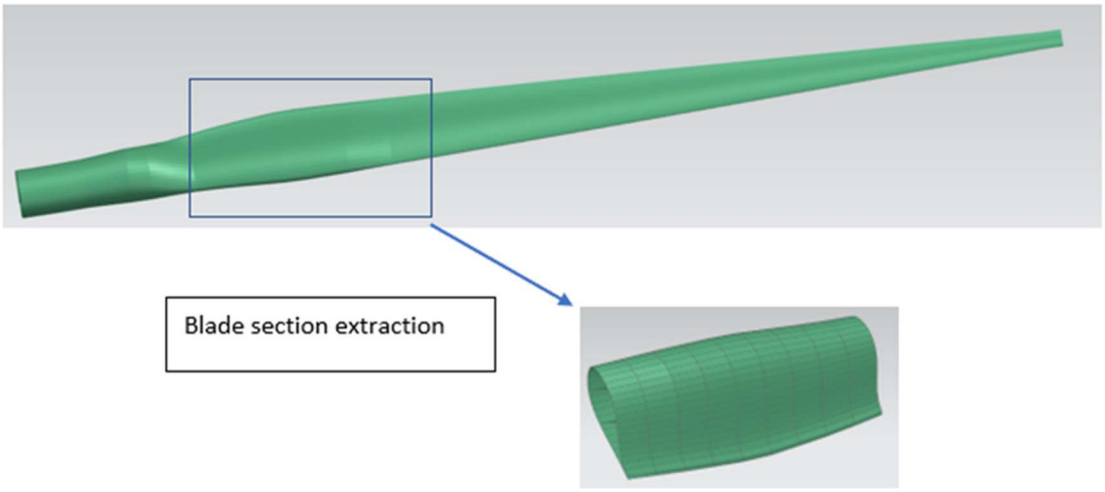

Figure 42: creation of the shell model of a part of the blade

From the full model of the wind turbine, we can extract the relative displacement/rotation of the blade section at R1 and R2 for any time of the simulation and to apply those boundary condition to the shell model of the selected piece of blade and to perform an intermediate simulation to obtain the 3D deformed configuration of the selected blade part (Figure 43).

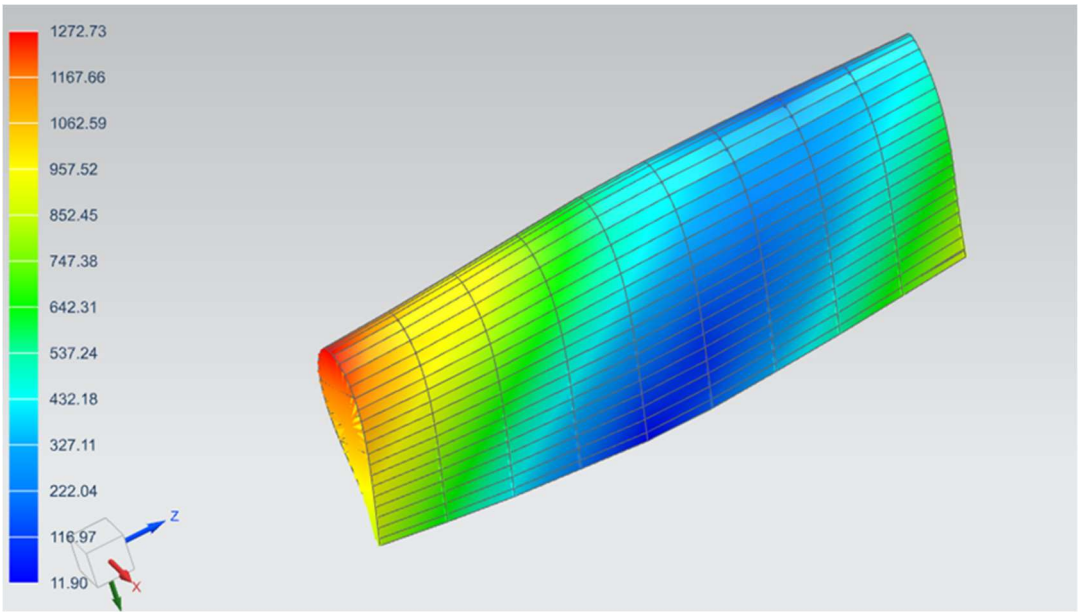

Figure 43: deformed configuration of the shell model of the thick part of the blade

The last step of the procedure consists in positioning the 3D composite model of the critical part of the blade. This is shown in Figure 44. This allow performing the zoom operation presented in [2] to obtain the boundary conditions applied to the 3D composite model.

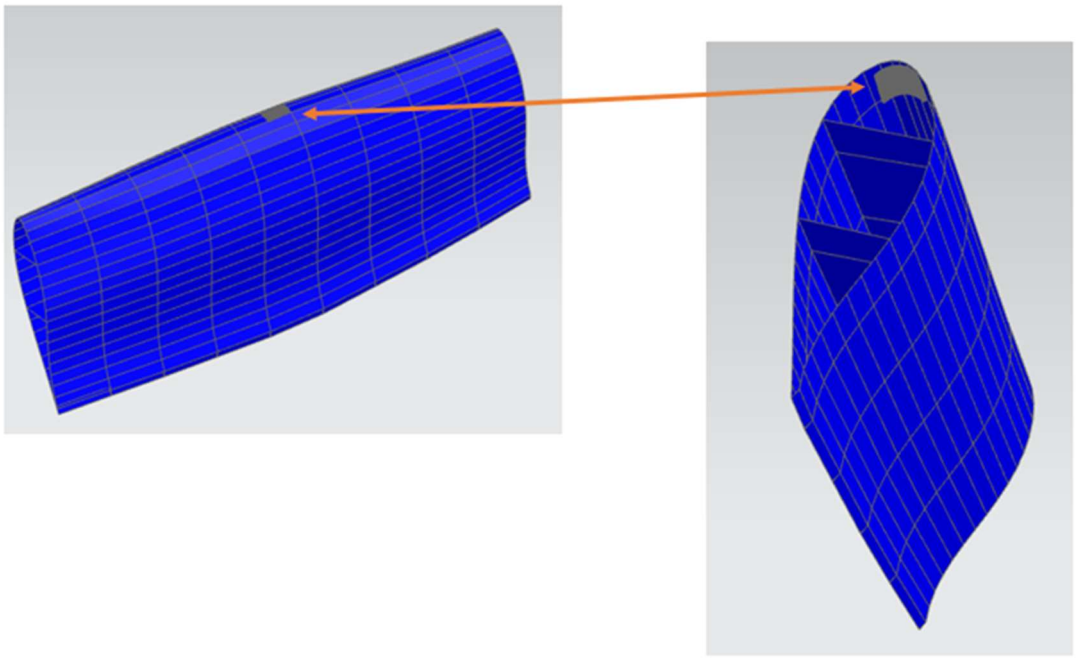

Figure 44: Positioning of the detailed 3D model inside the shell model

Figure 45 shows the obtained deformation of the detailed 3D composite model developed in the frame of WP5 [3]. The associated stress level is shown on Figure 46, where we can access stress levels in all composite plies and assess blade integrity considering fatigue damage model [4].

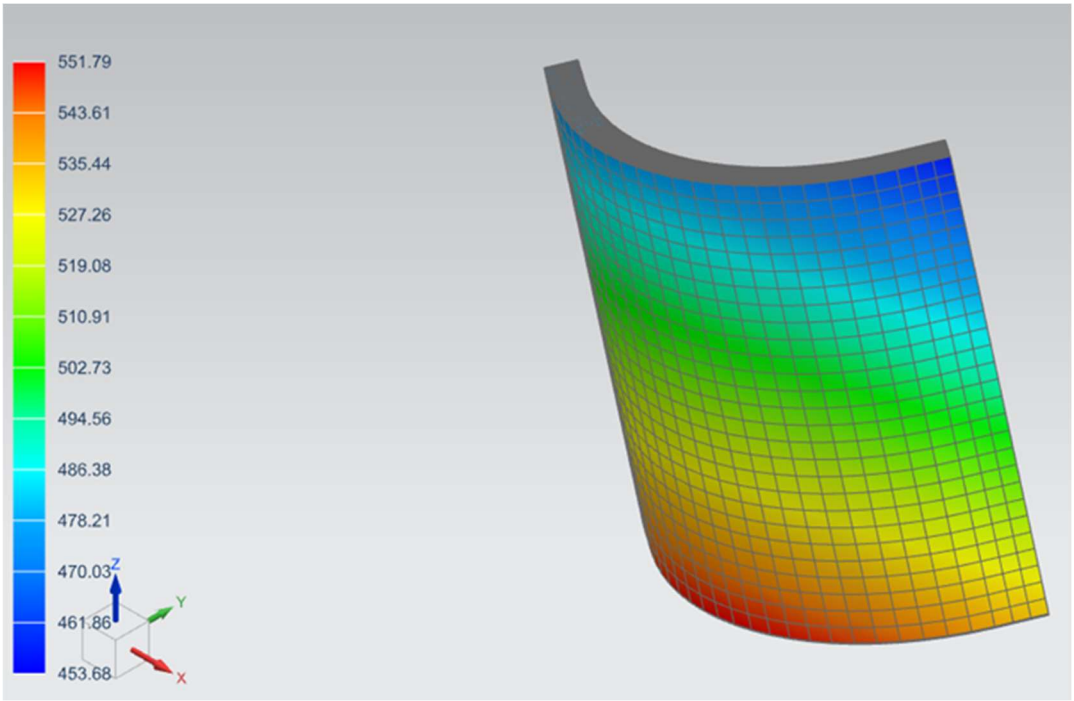

Figure 45: deformed local 3D model

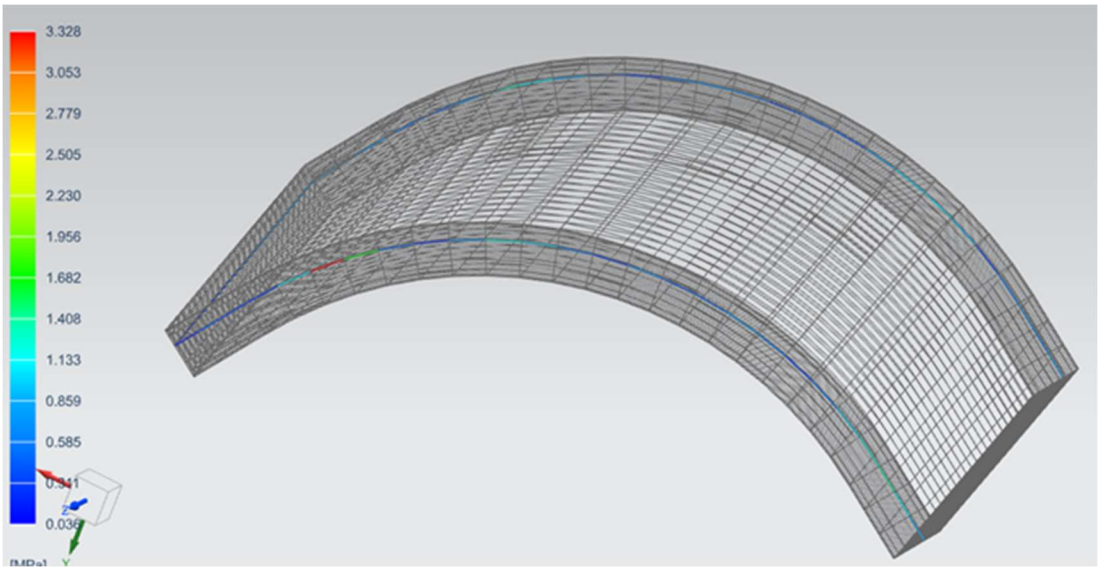

Figure 46: Local Von Mises stress in ply 20

Conclusion

In conclusion, the cosimulation reveals the effects of partial wake situation of turbines within a wind farm, not only on produced power but also on control behavior. Partial wake causes turbulences, which results in of load cycles of blade bending. This causes material stress on the blade composite material.

2.3. Study Case 1: Offshore analytics on Lillgrund

Similar to the workflow that was used for the Høg-Jæren Wind Farm, we used the Weather Research and Forecast system (WRF) to simulate atmospheric conditions covering wind direction and strength in the geo location of the offshore wind park Lillgrund. The main wind direction here was southwest. Thus, we rotated the WRF inlet window in order to conform to OpenFoam standards. Figure 47 shows the simplified wake model of the Lillgrund park.

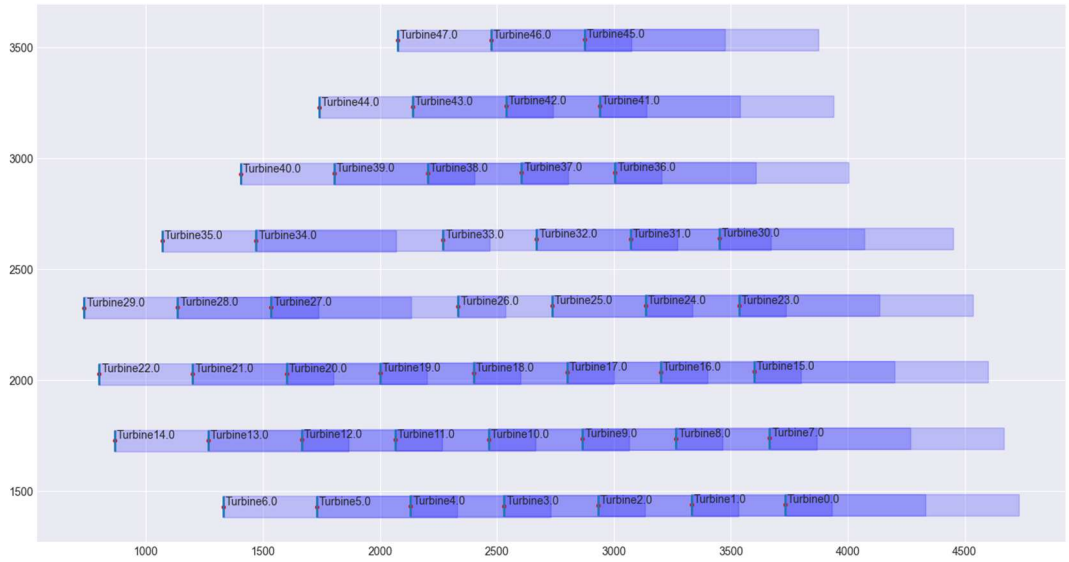

Figure 47: Simplified wake model of the Lillgrund wind park. The wind direction is from left to right.

The wind direction in Figure 47 is from left to right. Therefore, the turbines are located in rows with turbines 6, 14, 22, 29, 35, 40, 44 and 47 being in the freestream while the others are in the wake. Since the distances between rows are larger than those in the onshore case, we again consider the separate rows with no interactions in between. We have already gained some experience studying the Høg-Jæren Wind Farm, especially the information that a row-based yaw-controller can influence the produced power as well as the fatigue. Therefore, we used the same approach here, i.e., we conducted four simulations with varying yaw misalignments of the turbines in the freestream. These misalignments were -10°, 0, 5° and 10°.

In the following analysis we focus on the effect of the yaw misalignment on the power production. Here we also apply knowledge gained from the previous analysis.

Row analytics

First, we look at the power produced by the rows. Row 0 contains Turbines 0 to 6 while Row 7 contains Turbines 45 to 47. The other rows are numbered accordingly. The left part of the following Figure 48 shows the power produced by the different rows depending on the yaw misalignment of the turbines in the first column. The upper image shows the mean with respect to time while the lower image shows the variance. We consider these properties here because of the same arguments we used for the analysis of the onshore park. The colors encode the rows as follows:

- Row 0: Blue (Turbines 0 to 6)
- Row 1: Orange
- Row 2: Green
- Row 3: Red
- Row 4: Violet
- Row 5: Brown
- Row 6: Pink
- Row 7: Grey (Turbines 45 to 47)

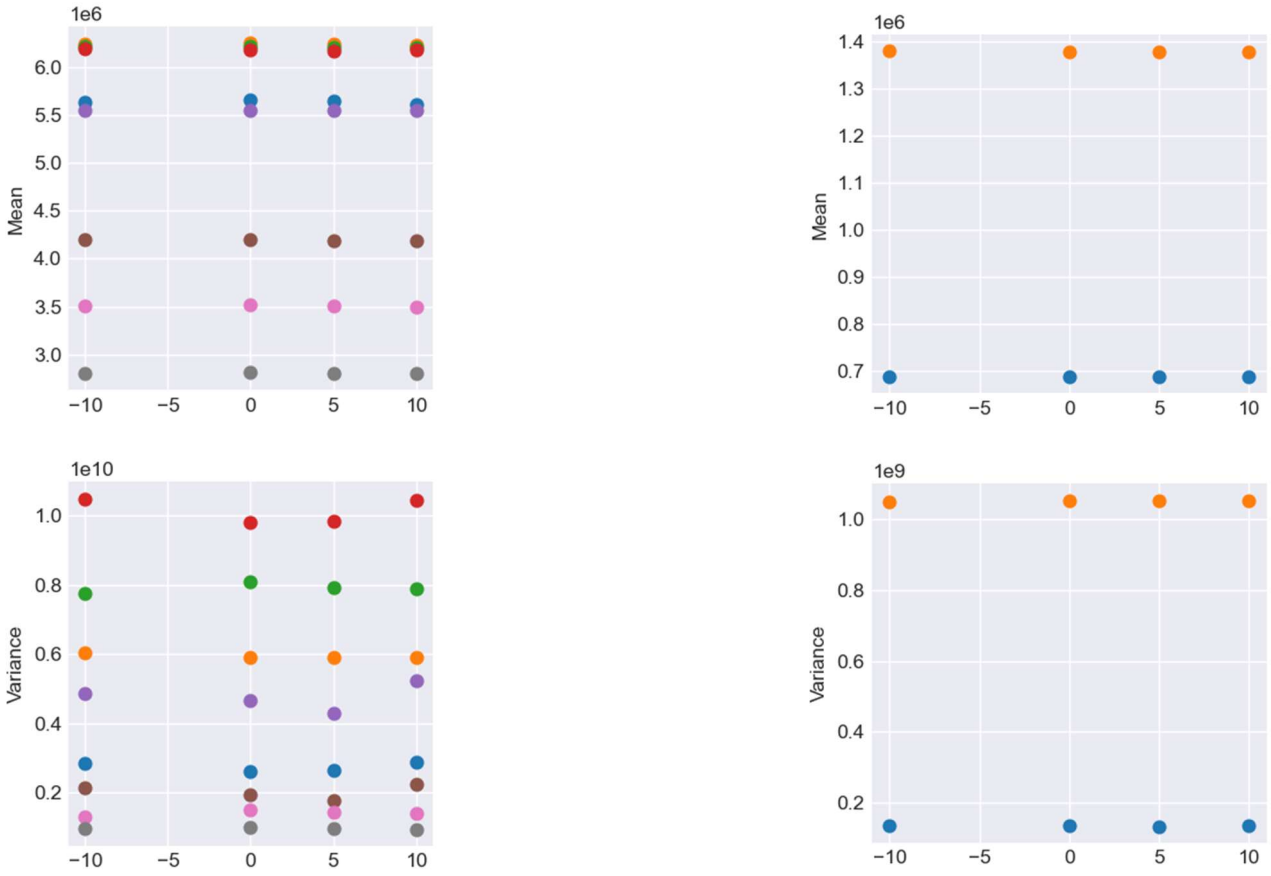

Figure 48: Left: The accumulated power produced by each row depending on the yaw misalignment. Additionally, the corresponding variance is displayed. Right: The power produced by Turbine 26 (orange) and Turbine 19 (blue) as well as the variance, also depending on the yaw misalignment.

As expected, the amount of produced power in each row is mainly determined by the number of turbines in that row. However, Row 3 (red) produces a similar amount of power as Rows 1 (orange) and 2 (green) while having one turbine less. This may be due to the rather large distance between turbines 26 and 27. The right figure shows that the power produced by turbine 26 is much higher than that of Turbine 19 despite them being the 4th turbine in their respective rows. Thus, the large distance between turbines 26 and 27 is accountable for the difference in produced power. One could draw the conclusion that less turbines with more distance between them perform similar to more turbines with less distance. Therefore, the cheaper option would be to have less turbines. However, the variance, which hints at the amount of stress that is put on the blades, is largest for Row 3. The variance in the produced power observed for Turbine 26 is much larger than the one for Turbine 19. Thus, less turbines with more distance in between may produce a high amount of power but the fatigue due to stress will also be significantly higher. One has to take both into account when looking for the optimal number of turbines and the optimal distances in a wind park.

Let us now consider the effect of yaw misalignment on the turbines. As examples we consider Rows 7 and 1 in depth. First, we take a look at Row 7 which contains Turbines 45, 46 and 47. We choose this row first, since it is similar to the onshore park where the maximum number of turbines in a row was 3. In Figure 49 the mean of the produces power and the corresponding variance for each of the three turbines is displayed. Similar to the findings of the onshore park, the produced power for turbines in the freestream (here Turbine 47) depend on the yaw misalignment in a nonlinear way. Again, the shape resembles a parabola. Turbine 46 which is situated in the wake of Turbine 47 behaves differently to what we saw in the Høg-Jæren park. There the dependence of the second

column on the yaw misalignment was approximately linear while it also is nonlinear here. However, in the Høg-Jæren case the downstream turbines face a partial wake situation while the turbines here face a full wake situation which explains this difference. The third turbine (Turbine 45) however displays a linear dependence which matches the findings from the onshore case.

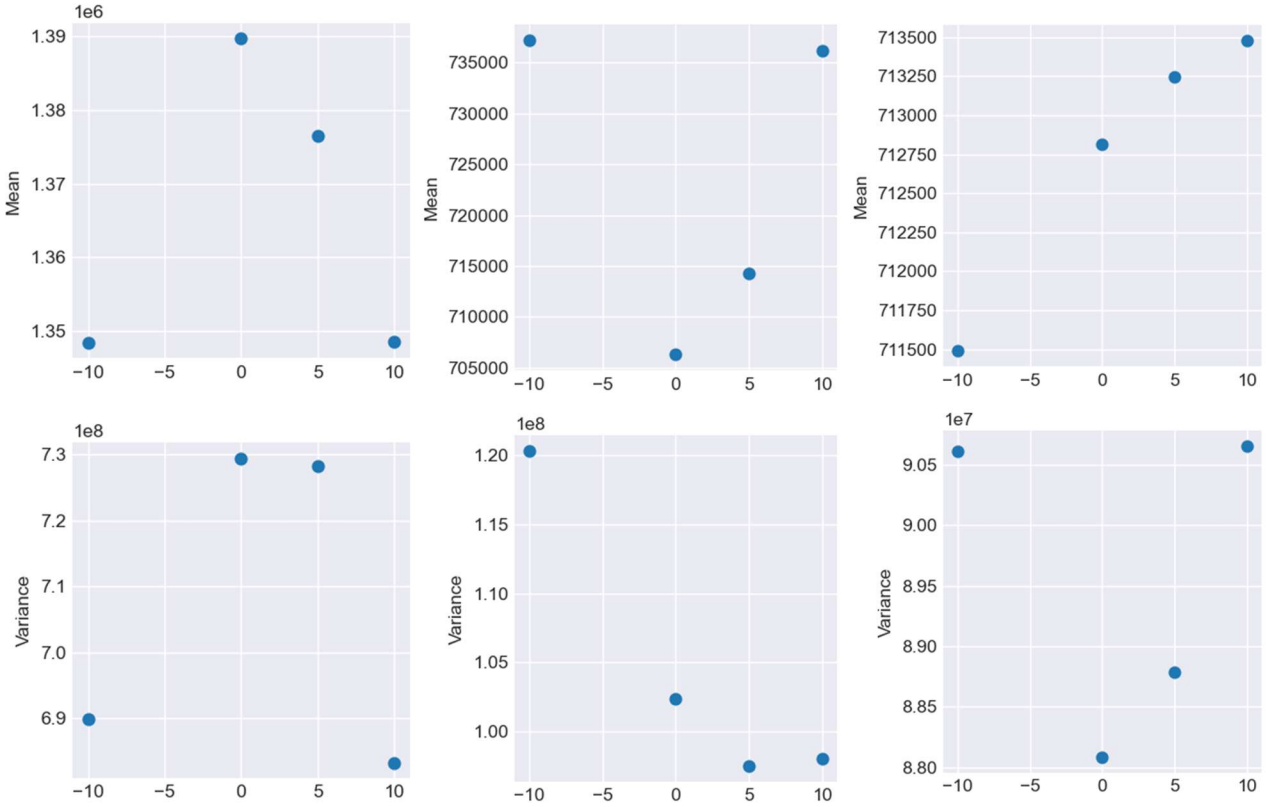

Figure 49: The mean of the produced power and the variance are displayed depending on the yaw misalignment. Left: Turbine 47, middle: Turbine 46, right: Turbine 45.

Figures 50 and 51 contain the same graphics for Row 1 (Turbines 7 to 14) in order to analyze a row with more turbines. We are especially interested in the behavior of the downstream turbines.

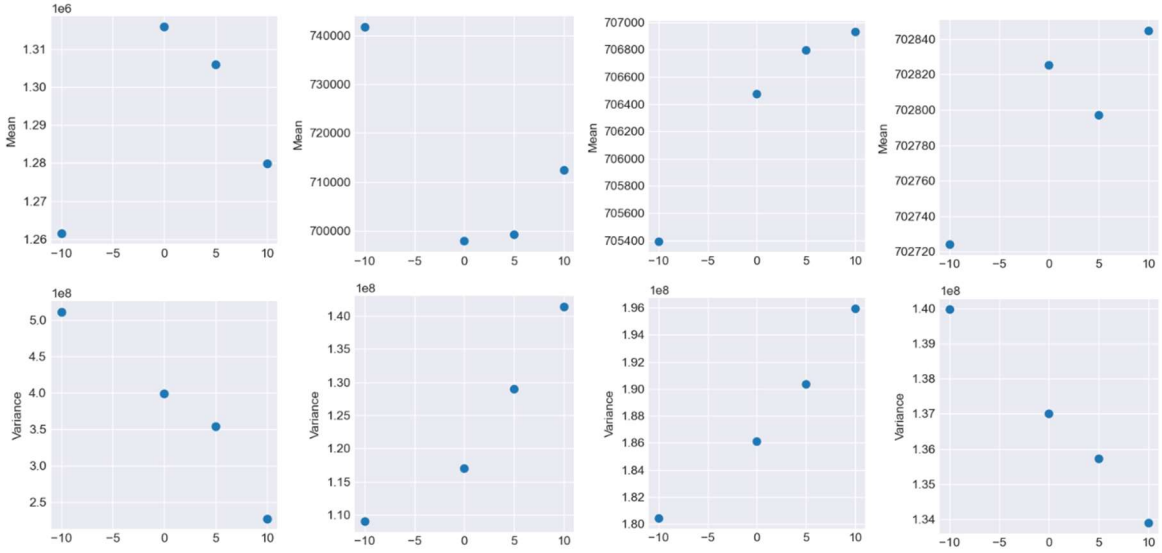

Figure 50: Mean of the produced power and the variance of different turbines in Row 1. From left to right: Turbines 14, 13, 12, 11.

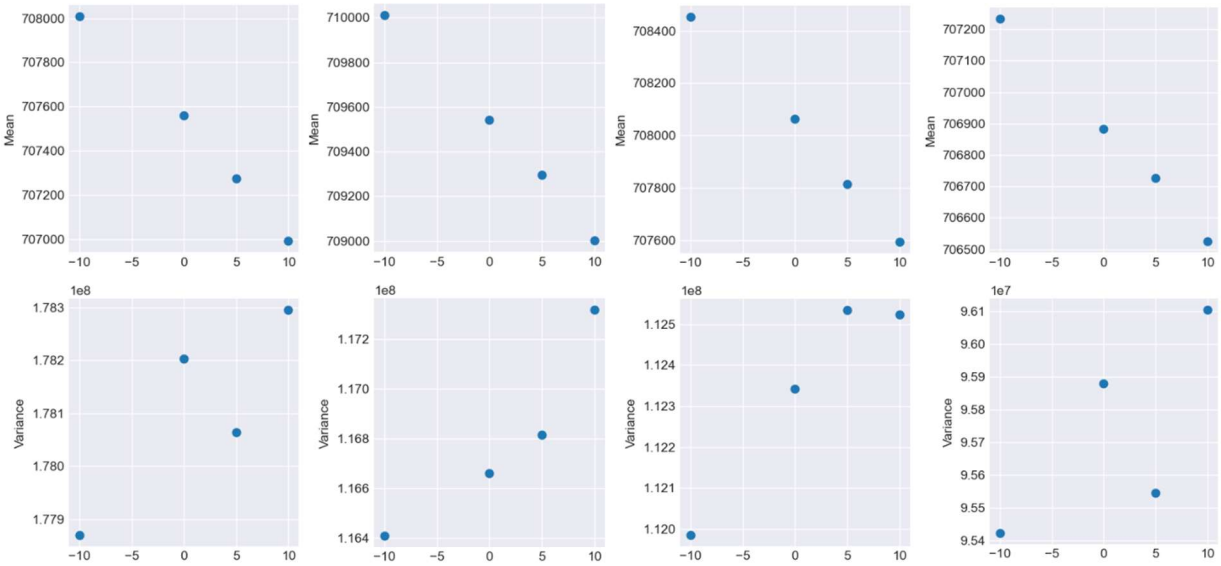

Figure 51: Mean of the produced power and the variance of different turbines in Row 1. From left to right: Turbines 10, 9, 8, 7.

The turbine in the freestream (Turbine 14) and the turbine in its wake (Turbine 13) again show nonlinear dependencies on the yaw misalignment when looking at the produced power. The other turbines display an approximately linear dependence. It is interesting to note that the slope of the linear dependence is positive for turbines 12 and 11 but negative for turbine 10 to 7. Further note the scale of the ordinate in the different images. The yaw misalignment has the largest effect on Turbine 14 in the freestream. The influence declines with the number of turbines that are in between the freestream and the considered turbine.

The variance is also highest for the first turbine. However, turbine 12 produces a higher variance of the produced power than turbine 13. The same goes for turbines 10 and 11.

In Figure 52 the power produced by Rows 7 and 1 is displayed as well as the variance. Since the number of turbines in Row 7 is three and the dependence on the yaw misalignment is largest for the turbine in the freestream, the behavior of Turbine 47 dominates the behavior of the row. The dependence of the produced power looks almost exactly like the dependence of Turbine 47. In contrast there are 7 turbines in Row 1, thus Turbine 14 does not dominate the produced power of the row as much. The dependence of the produced power on the yaw misalignment of the whole row does look different from that of turbine 14.

The variance in the produced power of one row is not as easy to interpret as the variance of every single turbine.

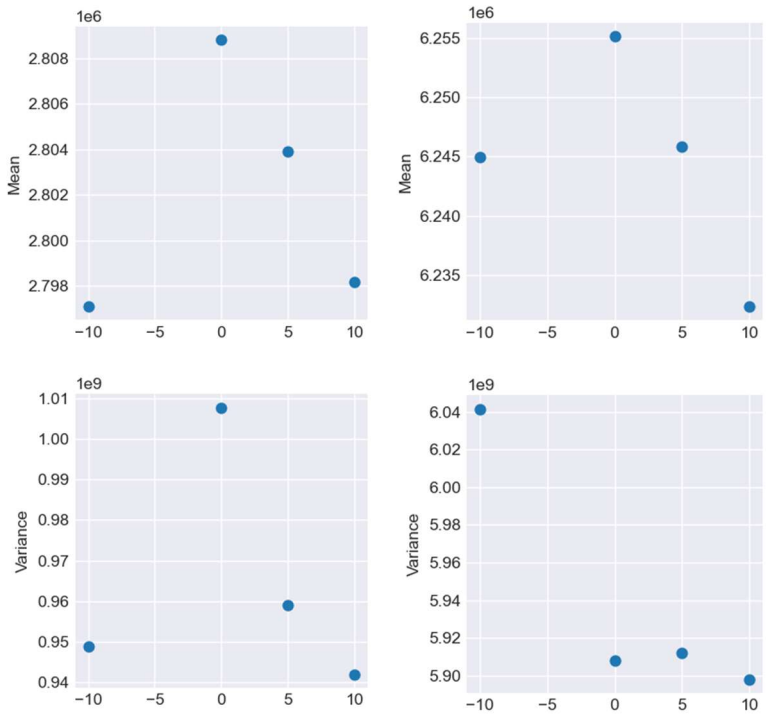

Figure 52: Accumulated produced power and corresponding variance of Rows 7 (left) and 1 (right).

Park analytics

Figure 53 shows the power produced by the whole park. As we have seen before, the turbine in the freestream has a large impact on the behavior of the row in terms of dependence of produced power on the yaw misalignment. However, like Row 1 the turbines in the wake do impact this behavior. Therefore, it is not surprising that the dependence of the produced power of the park on the yaw misalignment has a similar, but not the same, shape as the ones of the turbines in the freestream.

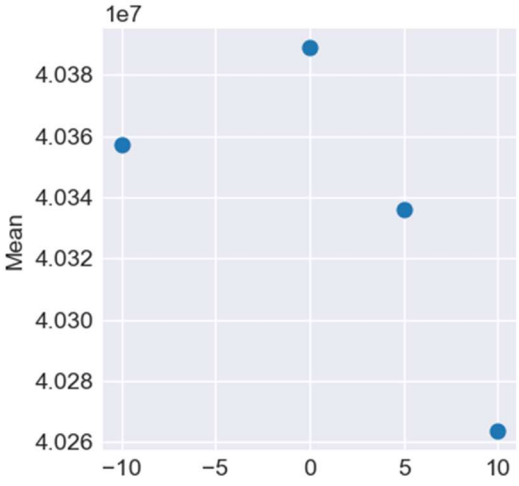

Figure 53: Mean value (with respect to time) of the produced power of the whole park.

Conclusion

In conclusion, the turbines in the offshore case behave similar to the ones in the onshore case when considering the dependence of the produced power on the yaw misalignment. A larger distance

between wind turbines leads to more produced power but also to more stress. A yaw controller of the first column of turbines can influence the produced power as well as the variance that hints at the amount of stress. If there are only few turbines in one row, it is sufficient to only look at the power produced by the first turbine when optimizing the yaw misalignment. If the number of turbines is larger, for example 7, a controller should also consider the turbines in the wake. However, a yaw misalignment around 0° seems optimal. Since the behavior is similar to the onshore case, it is possible that the optimal yaw misalignment is not exactly 0°. Remember that in the northwest case of the Høg-Jæren park the optimal yaw misalignment was slightly smaller than 0°.

2.4. Study Case 2: Onshore analyses on noise levels

In this study case, we investigate the effect of size and position of onshore turbines on emitted noise levels using the methodologies developed in WP4. The numerical workflow for wind turbine noise prediction is presented in Figure 54. It involves two main steps, namely the near-field and the far-field noise predictions.

In step 1, the prediction of trailing-edge broadband near-field noise of the wind turbine, due to the scattering of both suction and pressure side boundary-layers at the blade trailing edge, relies on a strip approach in which the blade noise is the sum of the acoustic fields generated by strips dividing the blade in the spanwise direction. The blade is cut at iso-radius stations, for which the flow around the blade section is obtained from two-dimensional Reynolds-Averaged Navier-Stokes (RANS) computations at the considered strips. The trailing-edge boundary-layer profiles are then extracted, and semi-empirical models are used to obtain the wall-pressure spectrum near the trailing-edge. Together with geometrical blade parameters, this constitutes the primary input to Amiet's theory for trailing-edge noise. In order to reproduce proper incoming flow conditions ingested by the wind turbine, an interfacing with the atmospheric flow model, in case of individual wind turbines, or with the park model, in case of wind farm is performed. This interfacing allows to take into account the flow non-uniformity due to the atmospheric boundary layer or to account for the wake interaction between the wind turbines of the wind farm. Further details about the near-field noise methods and interfacing with the Atmospheric and Park models are available in D4.2 and D4.5, respectively.

In step 2, the far-field sound propagation is calculated from a ray-based acoustic approach using the results of step 1 as sound sources. To this purpose, the Mithra calculation engine by CSTB is used. The propagation of sound between a source and a receiver is modeled as a 2-D problem in the vertical plane containing the source and the receiver. The intersection of this plane with the terrain topology forms the low boundary of the propagation domain, characterized by an acoustic impedance. In the propagation plane, the calculation engine takes into account the direct sound ray (if it exists) or the diffracted one (shielded by topography) as well as one or more rays reflected on the ground. It is worth noting that the reflections on the vertical obstacles (walls, buildings) as well as the diffraction around the vertical edges of these obstacles are considered negligible for the terrains under consideration and is not taken into account. In order to model the effects of the weather conditions on the sound propagation, the "Harmonoise" model, developed by CSTB, is used. Unlike standardized models whose primary objective is to predict averaged sound exposures over long periods of time, the Harmonoise model allows taking into account real, local and variable weather conditions over time. Further details on the coupling between the far-field propagation method and the atmospheric flow model are available in D4.2.

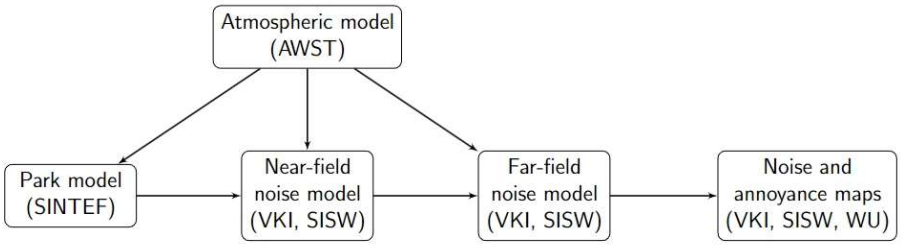

Figure 54: Noise prediction model coupled with Atmospheric and Park models.

Case study 2 focused on a subset of nine wind turbines located in the Høg-Jæren wind farm (see Figure 2). It is based on the park simulations of the south-east wind direction used in case study 1. Therefore, we focus on the effect that changing the yaw misalignment of the first turbines has on the produced noise. We considered yaw misalignments in the range $[-10°, 10°]$. The yaw angle case 0° is referred to as the baseline case in the following.

In Figure 55 below the overall sound pressure level (OASPL) in dB(A) is displayed as defined by the colorbar on a receiver grid located around the wind turbine park. In order to obtain a single value at a listener location on the grid, the sound spectrum resulting from the noise models is first corrected using an A-weighting that attempts to replicate how an average and normal ear would hear (Hansen et al., 2007), with a decrease of the perceived amplitude at low and high frequencies. The corrected spectrum is then integrated over the frequencies to obtain the overall sound pressure level (OASPL) at the receiver position. These OASPL iso-contours obtained for the south-east wind direction on the subset of the Høg-Jæren wind park are shown together with the noise regulations. The set-back distance is represented by the circles around the wind turbine locations and the purple line shows the convex hull created from the individual set-back distances, defined a global park set-back distance. The black iso-contour corresponds to the maximum allowable noise limit of 45 dB(A) as prescribed by the noise regulations in Norway. For the baseline yaw, minimum and maximum considered yaw angles, it is first noticed that the set-back distance is conservative compared to the noise limit of the regulations for the wind direction and amplitude for the case considered. The observer farm location (black cross in Figures 55 and 56) is positioned outside of the global set-back distance and noise limit, satisfying then the regulations in the present case. Depending on the yaw angle, the noise is produced by different wind turbines, showing the effect of the yaw angle on the wind turbine misalignment (for the upstream wind turbines) or on the wind turbine wakes impacting the downstream wind turbines. With a yaw angle of –10 degrees, the front wind turbines are shown to produce more noise due to the misalignment of the incoming wind. The sensitivity of the emitted noise seems to be reduced for the maximum yaw angle considered. This should be further investigated by looking at the individual wind turbine operating parameters and upstream wind conditions, and their link to the corresponding produced noise.

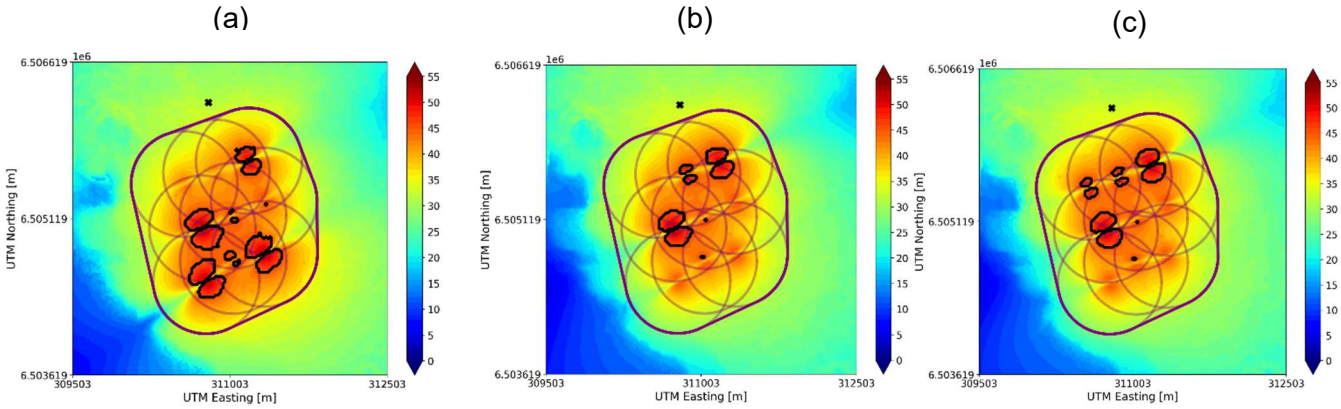

Figure 55: Output regulation maps of the noise simulation for (a) -10°, (b) 0° and (c) 10° of yaw misalignment.

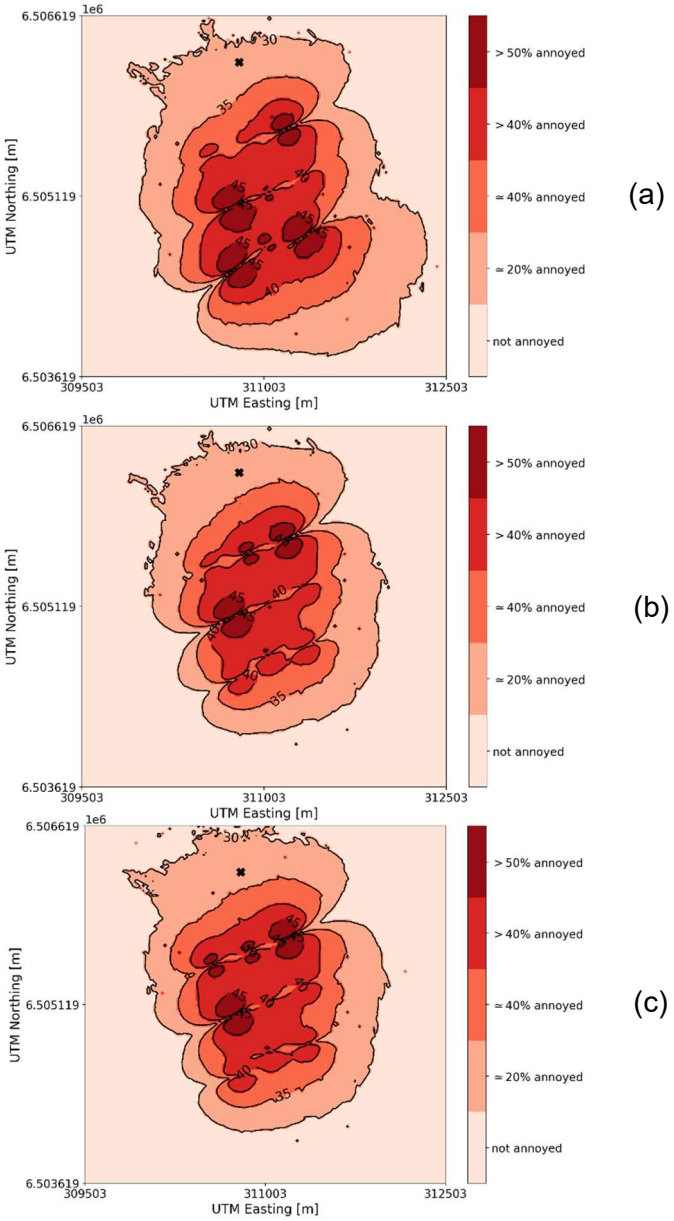

Figure 56: Annoyance maps for yaw alignment of (a) -10°, (b) 0° and (c) 10°

The corresponding annoyance maps obtained using a previous study performed in D7.2 are shown in Figure 56. As these iso-contours are a direct translation for the OASPL noise maps, the observed increase of noise amplitudes in Figure 55 are resulting in a larger area where people are likely to be annoyed. The yaw control then allows to possibly reduce the produced noise of a wind turbine park and its corresponding noise annoyance in its neighborhood.

For a particular observer position marked with the black cross in Figures 55 and 56, the OASPL is extracted for the different simulations performed in the yaw misalignments range, and reported in Figure 57. The noise is reduced by more than 2 dB(A) between the baseline configuration and the optimal configuration (obtained at -5° yaw misalignment), which is significant considering that a 3 dB(A) increase leads to doubling of the acoustic pressure on eardrums. No clear trend is observed over the yaw misalignment illustrating the complexity of the physical phenomena occurring in a wind farm, where the upstream wind alignment and wake interactions between the upstream and downstream wind turbines play an important role on the noise produced. The possible resulting model is then difficult to define using low-order regressions and would deserve more investigations to consolidate the obtained results.

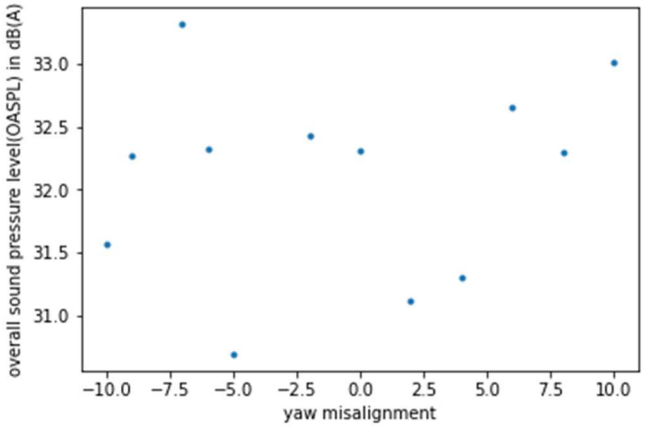

Figure 57: OASPL at the location indicated by the black mark in Figure 49 depending on the yaw misalignment of the first turbines.

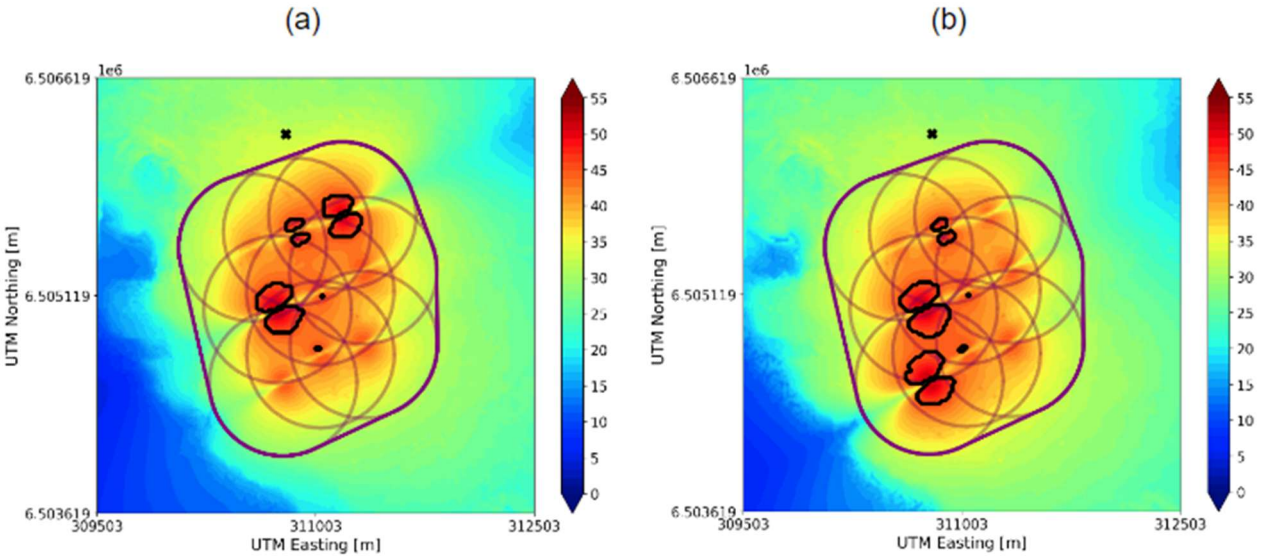

Figure 58: OASPL in dB(A) and noise regulations for the area around the park. Yaw misalignment of the front turbines of (a) 0° and (b) -5°, being the minimal value of the considered simulations. The black cross at the top of the park marks the position of the farm.

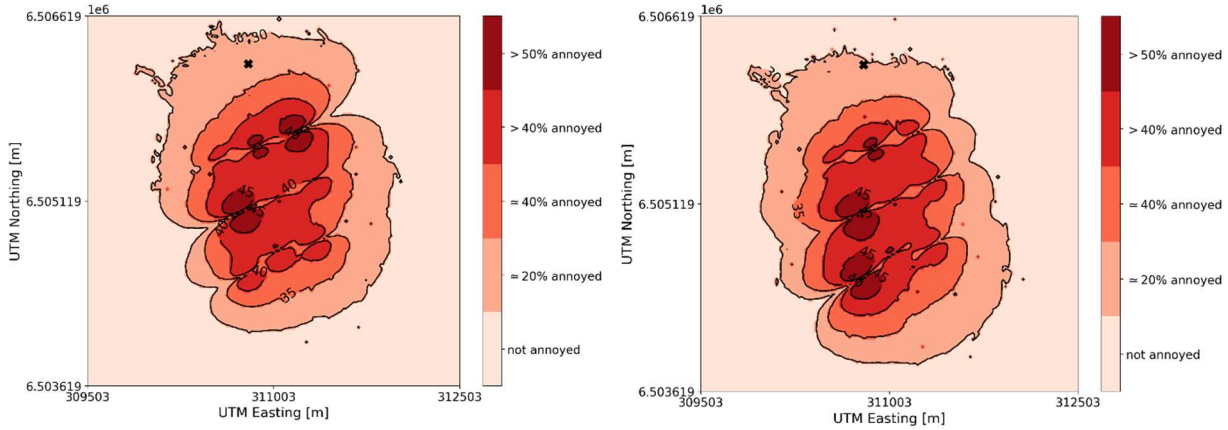

Figure 59: Noise annoyance maps for (a) 0° yaw misalignment (baseline case) and (b) -5° yaw misalignment (minimal OASPL)

The resulting noise footprints are further analyzed for the baseline and optimal park configurations in Figures 58 and 59. Figure 58 shows the OASPL iso-contours obtained for the south-east wind direction on the subset of the Høg-Jæren wind park, together with the noise regulations. Again, it is first noticed that the set-back distance is conservative compared to the noise limit of the regulations for the wind direction and amplitude for the case considered. The observer at the farm location is positioned outside of the global set-back distance and noise limit, satisfying then the regulations in the present case. When the optimal yaw angle for the noise reduction is used, the wind turbines close to the observer farm are seen to produce less noise, resulting in a noise decrease at the observer. This is probably due to an optimal arrangement of the upstream wind turbine wake impacting the last row of the wind park, reducing the rotational speed of the wind turbine or allowing a better flow uniformity over the rotor. Again, this should be further investigated by looking at the individual wind turbine operating parameters and upstream wind conditions, and their link to the corresponding noise produced.

Figure 59 shows the corresponding annoyance maps obtained using a previous study performed in D7.2. For the present park layout at yaw misalignment of 0°, wind amplitude and direction, about 20% of people are likely to get annoyed by the noise produced at the location of the observer farm (black cross on top). With a yaw misalignment of -5° (optimal yaw angle), this percentage drops to about 0%, making a substantial difference to the people's annoyance. It should be also noticed that despite the fact that regulations are satisfied at the observer farm, the percentage of people likely to be annoyed is not negligeable, showing that the regulations in place might not be sufficient to ensure a reduced annoyance in all cases.

Conclusion

The present case study showed the possibility to use the developed UPWARDS multi-physic platform to perform a yaw misalignment study on a subset of a wind farm. The results showed that an optimal noise production can be obtained at a single observer position by adapting the yaw angle of the front row of the wind farm, thanks to an improvement of the aerodynamic of the wind turbine rotors reducing noise sources. Even if this study case only tackles a reduced number of control parameters of the wind farm, the extension to an overall optimization of the wind farm is possible with the available platform and would result in an optimal wind farm layout and control allowing a minimal noise production for a maximal produced power.

2.5. Study Case 3: 15 MW turbines

In Study Case 3, we analyze the influence of slender design of large blades (15 MW) on the study of high-fidelity wind structure interaction, featuring strong coupling between state-of-the-art CFD and non-linear structural & multi-body analysis.

A summary of the geometrical and operational characteristics of the Siemens 15 MW wind turbine can be seen in Table 1.

Model	SWT 15MW
Number of blades	3
Blade length	112 m
Tower length	150 m
Prebend	2860 mm
Cone angle	2.5°
Tilt angle	7.5°
Rated rotor torque	16300000 Nm
Rated power	15000000 W
Rated speed	8.8 RPM

Table 1: Construction and operating data for the SWT 15 MW wind turbine

Aerodynamic Model

Due to the turbine's own movements (rotation and deformations) a meshing scheme must be used which involves:

- A sliding mesh, to make a disc-cone around the rotor and follow its rotation.
- A deformable mesh, used inside the disc-cone, to adapt the fluid mesh to the deformation and pitching of the blades.
- For the rest of the domain, a fixed mesh is used, which contains the tower and the nacelle.

The fixed mesh is of the deformable type; however, as the tower and the nacelle are considered rigid, the displacements of these bodies are set to zero throughout the simulations.

On the blade surfaces, the mean cell size is 0.03m. This dimension was adopted after performing a mesh convergence analysis. In the rest of the moving disc, the cells have a mean size of 0.4m. To generate the 3D mesh of the fluid, the Simcenter STAR-CCM+ program was used, based on the surface meshes (STL) obtained in the modelling of the structure using the BNREL program described in previous reports.

CFD detailed modelling of such very large wind turbines poses severe restrictions from the computational point of view for different reasons:

- The fluid mesh size over the blades is imposed by the necessity to represent certain aerodynamic features and cannot be much larger than the mesh size used for smaller wind turbines. In this case a mean cell size of 0.03m was used.
- The blades being much larger, the number of cells is therefore largely increased. Also, they can develop very large displacements at the tip, and for this reason the size of the rotating

mesh box has to be increased. In this case, a cone was used to be able to contain the morphing mesh that follows the blades deformation and still clear the tower.

- These difficulties mean that the total number of cells required to correctly represent the flow acting on a large wind turbine has to be increased with respect to other cases. In this example, a total number of about 20 million cells was used, but more cells would have been required for accuracy reasons. These constraints impose the use of important computational resources.

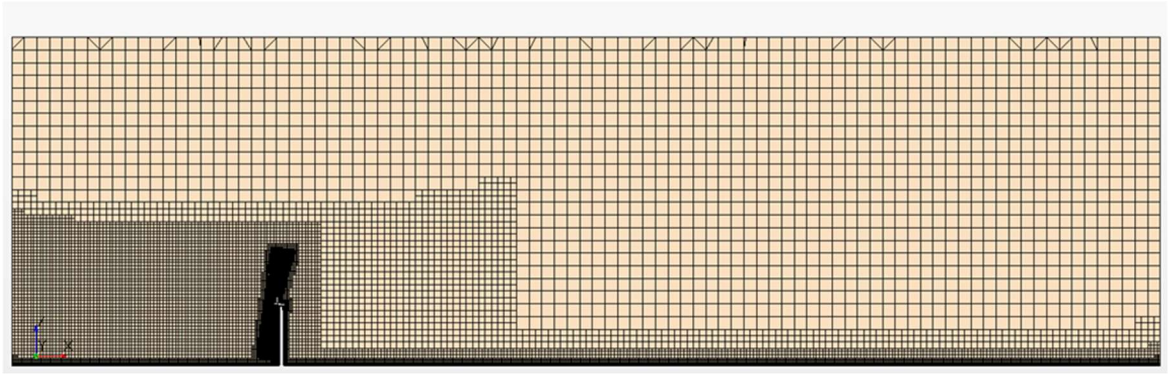

Figure 60: Lateral cut of the CFD mesh

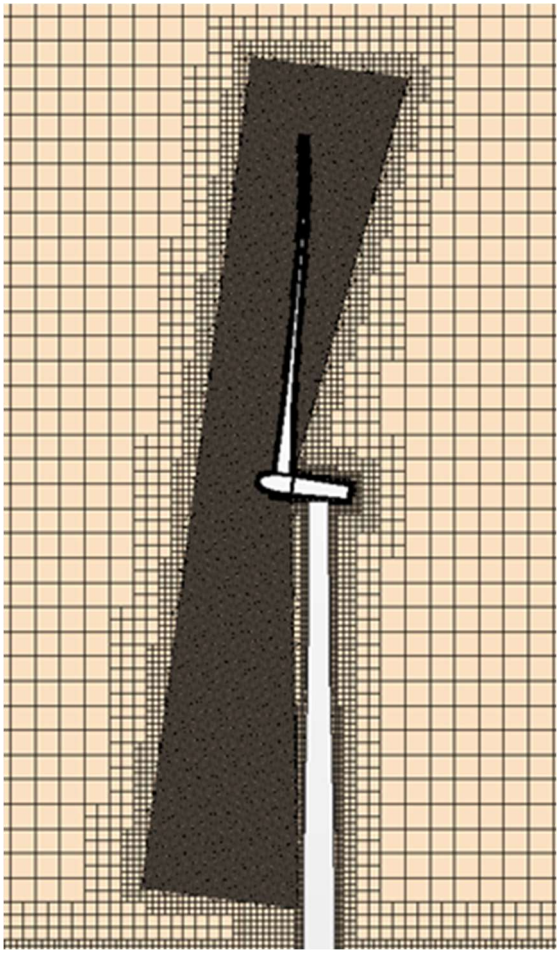

Figure 61: Disc-cone mesh detail allowing blade deflections while still clearing the tower

Initial and Boundary Conditions

In the fluid, in order to correctly model the physics over the turbine region and the floor of the control volume, a wall-type boundary condition is used. A symmetry condition is imposed on the side walls.

On the outlet side, a zero-outlet pressure condition is set. On the inlet wall, two inlet wind conditions were evaluated: on the one hand constant wind and on the other hand variable wind.

For the constant wind condition at the inlet, a velocity per component is imposed: in the X direction, the adopted values were 15 m/s and 12,7 m/s. The initial condition over the entire control domain corresponds to the chosen velocity.

For the variable wind condition, a time-varying atmospheric boundary layer (ABL) is imposed at the inlet. The average profile corresponds to a "suburban" type terrain (Bre and Gimenez, 2022) with Uref=15 m/s at the height of the rotor centre. The time series data, which considers a turbulent intensity I=0.4, is generated by means of the TurbSim tool (Jonkman et al., 2007). To generate the initial condition the velocity profile is advected in the domain. The data is entered into Simcenter STAR-CCM+ via a user library.

In the structural part, the pitch control angle is initially set at a zero value. The initial rotation velocity is imposed on the rotor as described in the start-up strategy section of the previous reports. The total simulation time for both runs is 22 s, with a time step of 0.01 s, 1 iteration of Simcenter Mecano–STAR-CCM+ exchange is used, 5 fluid iterations are needed for convergence per time step. The problem was solved in a parallel environment, with one process for Mecano and 64 processes for STAR-CCM+.

Simulation

In Figure 62, we display results for the constant wind condition with 12,7 m/s, and the other results are shown elsewhere (see D3.6). The rotor speed is set to the rated value, 8.8 rpm in this case. The blades are deformed by the actions of wind aerodynamic pressure, centrifugal loads and gravity. A maximum tip displacement of 24 m is predicted. A uniform, periodic pattern can be seen.

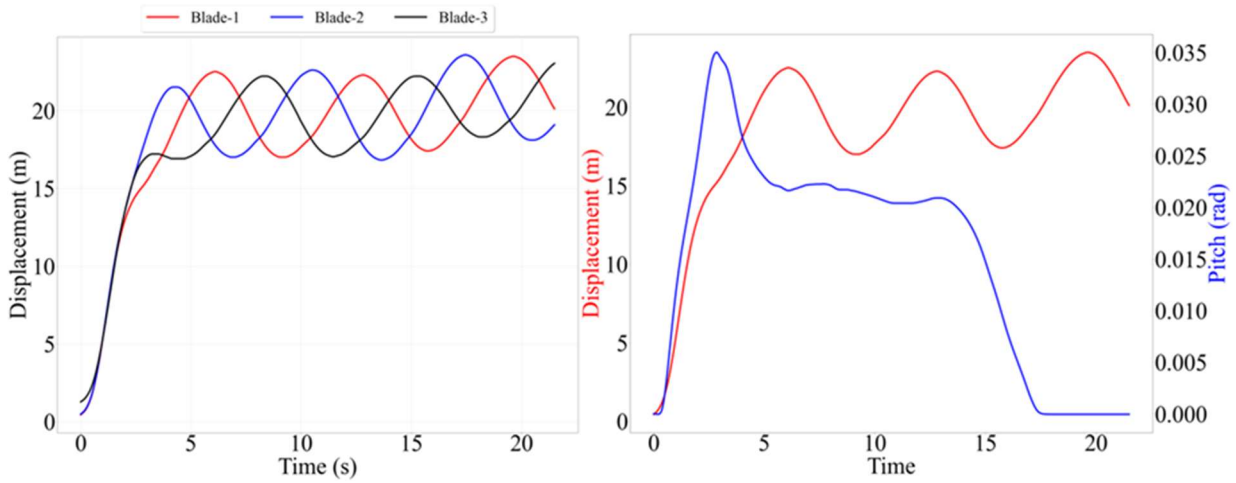

Figure 62: Tip displacements for the 15 MW wind turbine. The pitch is set at zero by the controller.

The displacements are maximal when the pitch is zero. This condition corresponds to that of maximum power generation of the wind turbine.

Next, Figure 63 shows the time evolution of the rotor speed. The target value is 0.921 rad/s and the model stabilizes (after an initial transient) at 0.916 rad/s.

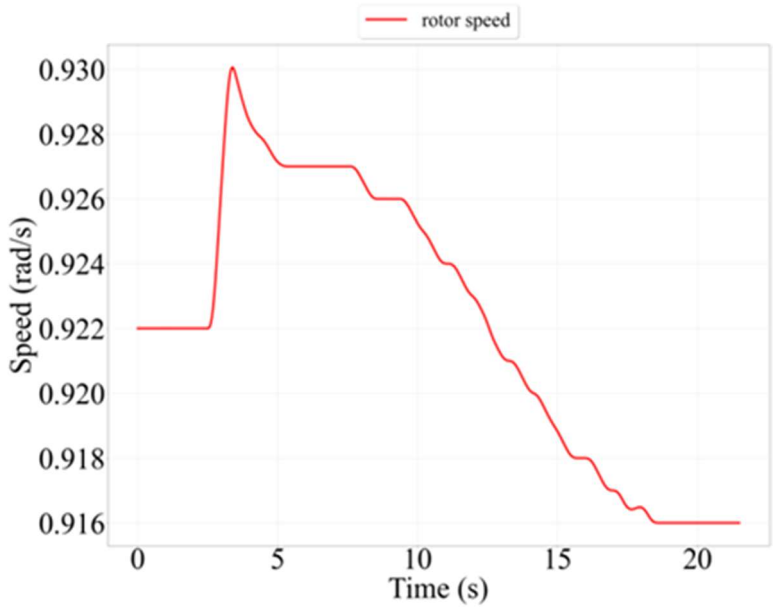

Figure 63: Rotor speed evolution

The time evolution of the generated power and thrust can be seen in Figure 64. These values are considered close to nominal.

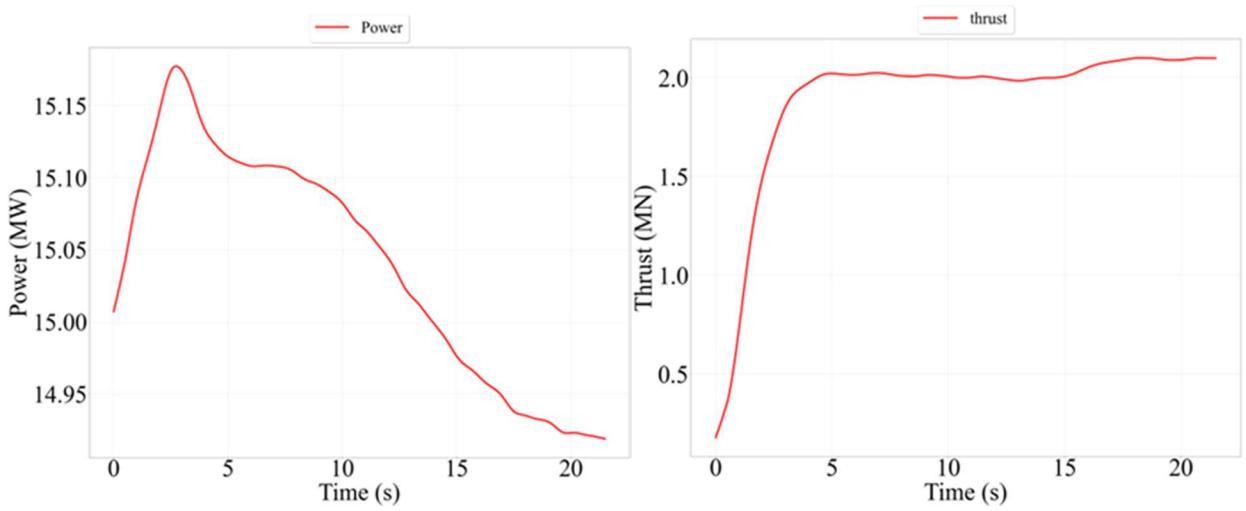

Figure 64: Evolution of power and total thrust on wind turbine.

We show next an XZ cut of the wind profile, and a visualization of the generated vortices on the wake (Q criterion).

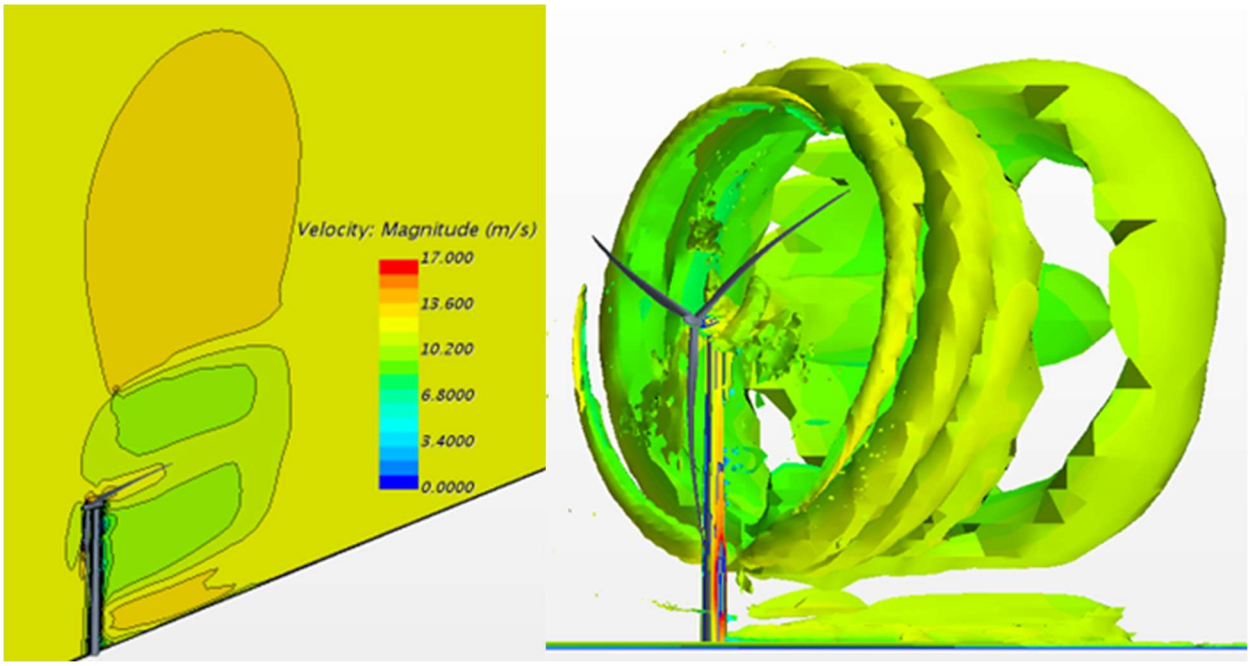

Figure 65: XZ cut of wind profile and vortices behind WT (Q criterion)

Conclusion

The WT industry is still exploring the blade design limits towards a – yet unknown – consensus on offshore WT size. The blade size challenges, directly related to very large deflections, are complex and multi-disciplinary in nature: aero-elasticity issues, complex structural and material failures, control interactions, structural dynamics design. The industry is always looking for new improved tools to push the state-of-the-art barriers without compromising the safety of the infrastructure. A multi-disciplinary high-fidelity tool-chain like the one developed in UPWARDS, and demonstrated in this Study Case 3, responds to this need.

As can be seen in the above sections, to achieve this successfully, a series of pragmatic approaches and actions were taken. We have shown that the very large displacements resulting from the design of slender large blades modify the blade response and interaction with the wind. This factor produces complex phenomena which should be taken into account in the analyses. Besides, the CFD modelling of these blades requires the use of very large computational resources as the mesh sizes should be increased to reproduce the interaction of the blades with the wind and to follow the complex behavior of the air passing through the wind turbine. The analyses have shown that high frequency oscillation patterns can be produced which are at the origin of fatigue phenomena, and these oscillations do not necessarily appear at the position of higher loading over the blades. For this reason, a complete analysis covering multiple operating states is needed.

3. Summary and Conclusion

In this document we described three case studies that were conducted using the integrated simulation framework developed in the Upwards project (refer to Figure 1). The goal was to use multi physical simulations to study the complex coupled phenomena of wind energy engineering.

In Study Case 1 the effect of changing the yaw misalignment (difference between the wind direction and the nacelle position of the turbine) of certain turbines on wake, turbulence, productivity and fatigue is considered. Both an onshore and an offshore park are used for this examination. The results could for example be used to design a yaw-based controller.

Study Case 2 deals with the effect of yaw misalignment in an onshore park on the noise level in the neighborhood. The results are used in Deliverable 7.3 where they are analyzed with respect to stakeholder needs. This can help increase the acceptance of wind parks.

In Study Case 3, the influence of slender design of large blades of a 15 MW turbine is studied. Here the impacts of wind structure interaction and non-linear bending on high-fidelity FSI computations are explored and pragmatic approaches are demonstrated to overcome the main issues.

The study cases revealed a potential in applying an active yaw control on park level to reduce turbulence effects on power, noise and stress caused by partial wake situations. For each target function (stress, power, noise), we could simulate park settings of yaw misalignments which enhance the overall park performance.

This shows the advantages and even the necessity of performing a multi physical end to end simulation of wind farms for dedicated geo locations.

4. References

- [D2.4] Final report on WRF-LES and Park coupling, Upwards Deliverable, Fraunhofer ITWM
- [D3.6] WT and Multi-Physics models validation with HPC domain decomposition, SINTEF
- [D6.1] Serial Integrated System Simulation Platform provided to partners, Upwards Deliverable, Fraunhofer ITWM
- [D6.2] Model Order Reduction Toolbox implemented, Upwards Deliverable, Fraunhofer ITWM
- [D6.3] HPC- Integrated Simulation Environment implemented and tested, Upwards Deliverable, Fraunhofer ITWM
- [D6.4] HPC-Framework Machine Learning implemented, tested and ready to use
- [D6.5] Virtual wind turbine prototype description, SINTEF
- [D6.6] Results from study cases applying integrated simulation framework, Upwards Deliverable, Fraunhofer ITWM
- [D7.3] Key features determined with machine learning, Upwards Deliverable, Fraunhofer ITWM
- V Leble and G Barakos, Forced pitch motion of wind turbines, 2016 J. Phys.: Conf. Ser. 753 022042
- Jonkman, B. and Jr, Buhl. TurbSim User's Guide. DOI 10.2172/15020326, 2007
- *C. H. Hansen, C. J. Doolan, and K. L. Hansen. Wind farm noise: measurement, assessment, and control. John Wiley & Sons, 2017.*